ACS OMEGA

Article

http://pubs.acs.org/journal/acsodf

Biosynthesized Protein-Capped Silver Nanoparticles Induce ROS-Dependent Proapoptotic Signals and Prosurvival Autophagy in Cancer Cells

Leena Fageria,[†,§] Vikram Pareek,[†,§] R. Venkataramana Dilip,[†] Arpit Bhargava,[†] Sheik Saleem Pasha,[‡] Inamur Rahaman Laskar,[‡] Heena Saini,[†] Subhra Dash,[†] Rajdeep Chowdhury,[*,†] and Jitendra Panwar[*,†]

[†]Department of Biological Sciences and [‡]Department of Chemistry, Birla Institute of Technology and Science, Pilani 333031, India

Supporting Information

ABSTRACT: In recent years, the use of silver nanoparticles (AgNPs) in biomedical applications has shown an unprecedented boost along with simultaneous expansion of rapid, high-yielding, and sustainable AgNP synthesis methods that can deliver particles with well-defined characteristics. The present study demonstrates the potential of metal-tolerant soil fungal isolate *Penicillium shearii* AJP05 for the synthesis of protein-capped AgNPs. The particles were characterized using standard techniques, namely, UV−visible spectroscopy, transmission electron microscopy, X-ray diffraction, and Fourier transform infrared spectroscopy. The anticancer activity of the biosynthesized AgNPs was analyzed in two different cell types with varied origin, for example, epithelial (hepatoma) and mesenchymal (osteosarcoma). The biological NPs (bAgNPs) with fungal-derived outer protein coat were found to be more cytotoxic than bare bAgNPs or chemically synthesized AgNPs (cAgNPs). Elucidation of the molecular mechanism revealed that bAgNPs induce cytotoxicity through elevation of reactive oxygen species (ROS) levels and induction of apoptosis. Upregulation of autophagy and activation of JNK signaling were found to act as a prosurvival strategy upon bAgNP treatment, whereas ERK signaling served as a prodeath signal. Interestingly, inhibition of autophagy increased the production of ROS, resulting in enhanced cell death. Finally, bAgNPs were also found to sensitize cells with acquired resistance to cisplatin, providing valuable insights into the therapeutic potential of bAgNPs. To the best of our knowledge, this is the first study that provides a holistic idea about the molecular mechanisms behind the cytotoxic activity of protein-capped AgNPs synthesized using a metal-tolerant soil fungus.

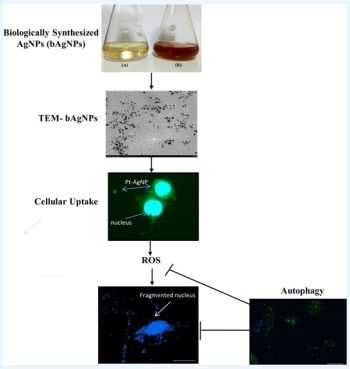

INTRODUCTION

In recent years, nanoparticles (NPs) have emerged as a novel class of materials with potential for a wide range of biomedical applications.[1] The intrinsic nature of NPs, such as their ability to absorb or carry other compounds and their ease of cell penetration has made them potentially useful, especially, in the biomedical field. In spite of tremendous advances in the use of nanomaterials in diagnostics, therapy, and healthcare, the key challenges involve determining how to get these advances to the clinic.[2] Among various nanomaterials, silver NPs (AgNPs) have received considerable attention due to their unique properties such as conductivity, chemical stability, relatively lower toxicity, and outstanding therapeutic potential, such as anti-inflammatory, antimicrobial, and anticancerous activities.[3−5] Today AgNPs have widespread biological applications and the highest level of commercialization among nanomaterials.[6] Silver has been known to be used since ancient time as an antimicrobial agent, as a component of dental alloys, and for preservation and decoration of sweets and other food materials. It has been demonstrated that at low concentrations, AgNPs are nontoxic to human cells.[7] However, the associated potential toxicity in therapeutic applications has always been a cause of concern for their long-term use.[8]

Cancer has become one of the most dreadful diseases with ever increasing mortality rate worldwide. Traditionally practiced therapy with cytotoxic drugs alone or in combination with radiation is mostly ineffective in eradicating the disease. Tumor cells bypass the effect of chemotherapeutic insult by developing intrinsic or acquired resistance to the drugs. Additionally, there is a trauma of development of postchemotherapy side effects, which is very distressing to the patient and at times is fatal enough, enforcing mortality.[9] In this regard, NPs offer an attractive alternative to conventional chemotherapeutics. NPs have unique ability to home specifically into tumor tissues by utilizing their leaky vasculature by enhanced permeability and retention (EPR) effect.[10] This can enhance the anticancerous effect of the NPs if they are inherently cytotoxic or used as drug delivery vectors; also, simultaneously, this reduces systemic toxicity.

In recent years, the applications of AgNPs have risen up in cancer diagnosis and treatment.[5,11,12] Various reports demonstrated the cytotoxic effect of AgNPs against different cancer

Received: January 26, 2017
Accepted: March 17, 2017
Published: April 17, 2017

DOI: 10.1021/acsomega.7b00045
ACS Omega 2017, 2, 1489−1504

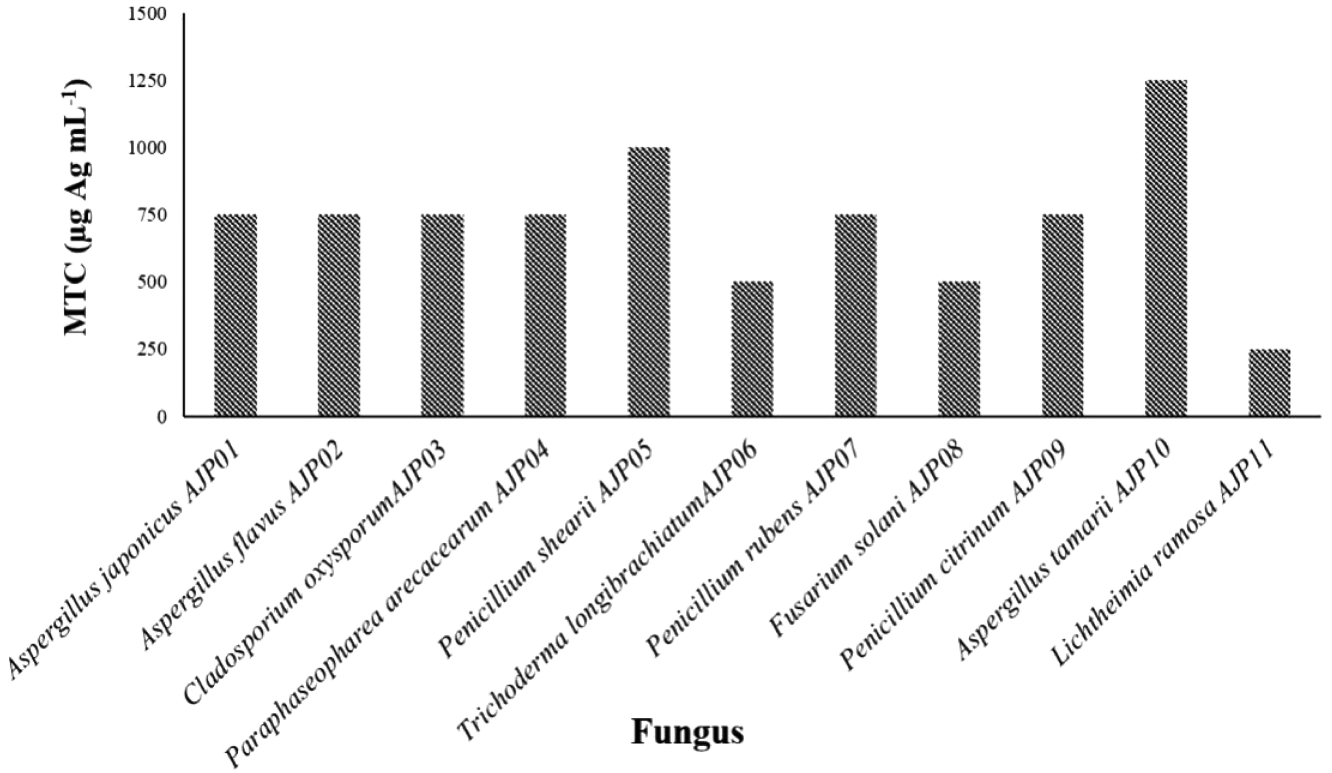

Figure 1. Silver metal tolerance profile of fungal isolates.

cells.[13−15] Reactive oxygen species (ROS) generation and DNA damage leading to mitochondria-dependent apoptosis have been considered as the possible mechanisms of AgNP-mediated cytotoxicity.[3,16] In general, the toxicity of AgNPs appears to be driven by the release of Ag^+ ions, which depends on the dissolution rate of AgNPs inside the cells.[5,17] Thus, a strict control over the release of Ag^+ ions is a prerequisite for the anticancerous efficacy of AgNPs. Surface coating or functionalization of NPs serves as the most important factor in this regard.[18] It has been reported that modification in surface properties can improve the cellular internalization of NPs while decreasing their possible side effects.[19,20] Furthermore, surface properties can affect the dispersibility of NPs in culture media and subsequently their cellular uptake and cytotoxicity profile. Thus, to understand the actual cytotoxic mechanism of NPs, it is necessary to have NPs together with reasonable controls of those key physicochemical properties.[21]

In recent years, extensive research has been carried out for the controlled synthesis of NPs. Most of the chemical and physical methods used are energy- and capital-intensive, employ toxic chemicals, and often yield particles in nonpolar organic solutions, thus, precluding their biomedical applications.[22] Microbial synthesis of NPs has recently emerged as a widely used approach for the production of biogenic NPs.[23] Among microorganisms, fungi are proven to be one of the most potential candidates for the extracellular synthesis of NPs due to their easy handling, inexpensive maintenance, and ease of downstream processing because of enormous extracellular secretary compounds. These biomolecules act as reductants and are found to have a significant advantage over their counterparts as protecting/capping agents.[24] Also, the extracellular protein secretions by fungi can be easily scaled up, leading to the development of so-called NP synthesis reactors.[25,26]

In the present study, opting the nature's own sustainable way of interacting with metal ions, indigenous metal-tolerant soil fungal isolates were utilized to develop an ecofriendly and low-cost protocol for the extracellular synthesis of AgNPs. The biosynthesized protein-capped silver NPs (bAgNPs) were further opted for investigating their biological functions, particularly anticancer effects, in comparison to those of bare bAgNPs and commercially available chemically synthesized silver NPs (cAgNPs). Cancer cells of two different origins, that is, epithelial (human hepatocellular carcinoma, HCC) and mesenchymal (human osteosarcoma, OS), were selected for the present study. It is well known that the response of cytotoxic drugs may vary according to the cell types. Hence, it is essential to confirm whether the cell-sensitizing potential of prospective compounds is true for cell types of varied origin. HCC is one of the most complex and aggressive cancer types. Around 80% of HCC patients worldwide are diagnosed at an advanced stage of the disease; the median survival of these patients is only 6−8 months. For the large number of patients, the choice of curative resection or ablation therapy remains practically nil and palliative treatment is the only preferred alternative.[27,28] OS, on the other hand, is the most prevalent primary malignant bone tumor that is very aggressive, which when untreated shows rapid local and systemic progression, leading to severe mortality. The 5-year survival rate of high-grade OS is as low as 20%. Despite exceptional local control through surgery, patients with even localized OS ultimately develop metastasis and die.[29,30] The surgical failure and associated necessity to find a cure led to the development of various multimodular chemotherapeutic regimes for the treatment of OS. However, in majority of cases, for both HCC and OS, the complex etiology of the tumor, highly variable biological behavior, and acquired resistance to chemotherapeutic drugs complicate the treatment, leading to eventual failure. This signifies the pressing

DOI: 10.1021/acsomega.7b00045
ACS Omega 2017, 2, 1489−1504

need to identify a repertoire of novel drugs that can be effective against such dreadful disease outcomes. Hence, the present study investigated the cytotoxic potential of the mycogenic AgNPs against HCC and OS cells in vitro. Results show that the fungal-derived protein-capped AgNPs have shown more cytotoxic effect than that of chemically synthesized or bared bAgNPs. This signifies the role of fungal-secreted materials in enhancing the cytotoxicity of the bAgNPs. The detailed mechanism of action of these mycogenic bAgNPs has also been investigated. To the best of our knowledge, this is the first report on the anticancerous effect of mycogenic protein-capped AgNPs and their detailed mechanism of action.

RESULTS AND DISCUSSION

Metal Tolerance Assay and Screening of Fungal Isolates. All of the fungal isolates were screened for their metal-tolerance ability against silver ions, and the results were expressed in terms of MTC (Figure 1). All fungal isolates were able to survive up to 250 μg mL^{-1} silver concentration. *Aspergillus tamarii* AJP10 (MTC: 1250 μg Ag mL^{-1}) was found to be the most tolerant fungus among all of the isolates followed by *Penicillium shearii* AJP05 (MTC: 1000 μg Ag mL^{-1}). A high proportion (>70%) of fungal isolates depicts significant silver-tolerance ability. All of the fungal isolates were screened to check their potential for extracellular synthesis of AgNPs. On the basis of the promising results for quick and efficient extracellular synthesis of AgNPs, *P. shearii* AJP05 was chosen for further studies.

Characterization of bAgNPs. The extracellular synthesis of AgNPs using the cell filtrate of *P. shearii* isolate AJP05 was monitored by the progressive change in color of the reaction medium. Figure 2 shows Erlenmeyer flasks containing the fungal cell-free filtrate without and with silver nitrate after completion of reaction at 50 min. The flask containing silver nitrate solution and fungal cell-free filtrate showed change in color of reaction mixture from colorless to brown during the incubation period. In contrast, no change in color was observed in the flask containing only the fungal cell-free filtrate. Moreover, the negative control (pure silver nitrate solution without cell-free filtrate) did not show any characteristic change in color, suggesting the importance of fungal cell-free filtrate in NP synthesis.

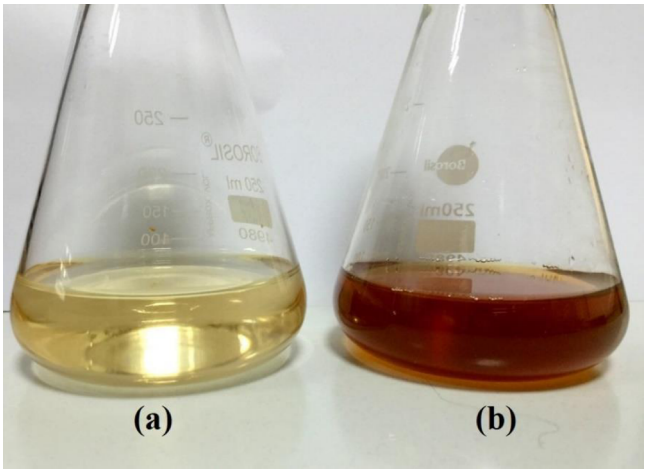

Figure 2. Erlenmeyer flasks containing cell-free filtrate of *P. shearii* isolate AJP05 without (a) and with (b) silver nitrate solution (1 mM) after 50 min of reaction.

The rate of NP synthesis was monitored using UV−visible spectroscopy, which has been considered as the most commonly employed technique for characterization of silver NPs. The absorption spectra showed a gradual increase in the absorption maximum peak at 446 nm with respect to time without any shift in the peak (Figure 3a). It was due to the excitation of surface plasmon, which is a typical phenomenon of noble NPs and indicates the presence of silver NPs.[39] No drastic increase in absorbance at 446 nm was observed after 50 min of incubation, indicating nearly complete reduction of precursor silver ions. The stability of NP solution was regularly determined by UV−visible spectroscopy up to 3 months, and the solution was found to be stable at room temperature with no flocculation. However, after removal of protein coating, agglomeration was observed in the bare NP solution. Hence, the bare NP solution was sonicated each time before use using a high-energy probe (100 W, 40 kHz) for 30 min to prevent agglomeration.

The morphology and shape of NPs were determined by TEM micrographs (Figure 3b), which revealed that the as-synthesized NPs were somewhat spherical in shape and uniformly distributed without significant agglomeration. The particle size histogram (Figure 3c) of AgNPs shows that the particle size ranges from 3 to 20 nm with an average size of 8.0 ± 2.7 nm. The frequency distribution suggests that almost 80% of the particles were in the 6−15 nm range.

The diffraction pattern of the drop-coated film of as-synthesized NPs showed well-defined peaks at 2θ values of 38.26, 64.71, and 77.38°, which correspond to the (111), (220), and (311) planes of silver, respectively (Figure 4a). These values were in accordance with the face-centered cubic (fcc) lattice structure of crystalline silver (JCPDS file no. 04-0783). A similar pattern of X-ray diffraction (XRD) spectrum has been previously reported by our group for silver NPs synthesized by *Aspergillus* sp.[18]

Characterization of Capping Materials of bAgNPs. The UV−visible absorption spectrum of the bare bAgNPs and supernatant of the SDS-treated bAgNPs showed absorbance peaks at 446 and 280 nm, respectively (Figure 4b). Noticeably, the bAgNP absorption spectrum also shows a peak around 280 nm, confirming the presence of proteins as the capping material on the NP's surface.

FTIR measurements of the bAgNPs were carried out to characterize the capping materials present on the surface of NPs. FTIR spectrum exhibited characteristic bands at wave numbers 1637 and 3268 cm^{-1} that correspond to the bending and stretching vibrations of the amide I bond, respectively (Figure 4c). This supports the UV−visible spectroscopy results, representing the presence of proteins on bAgNPs' surface as a capping material.

The capping materials isolated after treatment with 1% SDS solution in boiling water bath for 15 min were further resolved on SDS-PAGE using a 12% resolving gel (Figure 4d). Interestingly, the SDS-treated sample showing the presence of three bands of ca. 65, 55, and 50 kDa was observed (lane 3). These proteins were also present in the extracellular cell-free filtrate of *P. shearii* isolate AJP05, as shown in lane 2. Therefore, it can be proposed that the observed proteins act as a capping material and confer stability to silver NPs.

Biologically Synthesized AgNPs Induce Cytotoxicity in Cancer Cells. Because of unique physicochemical proper-

DOI: 10.1021/acsomega.7b00045
ACS Omega 2017, 2, 1489−1504

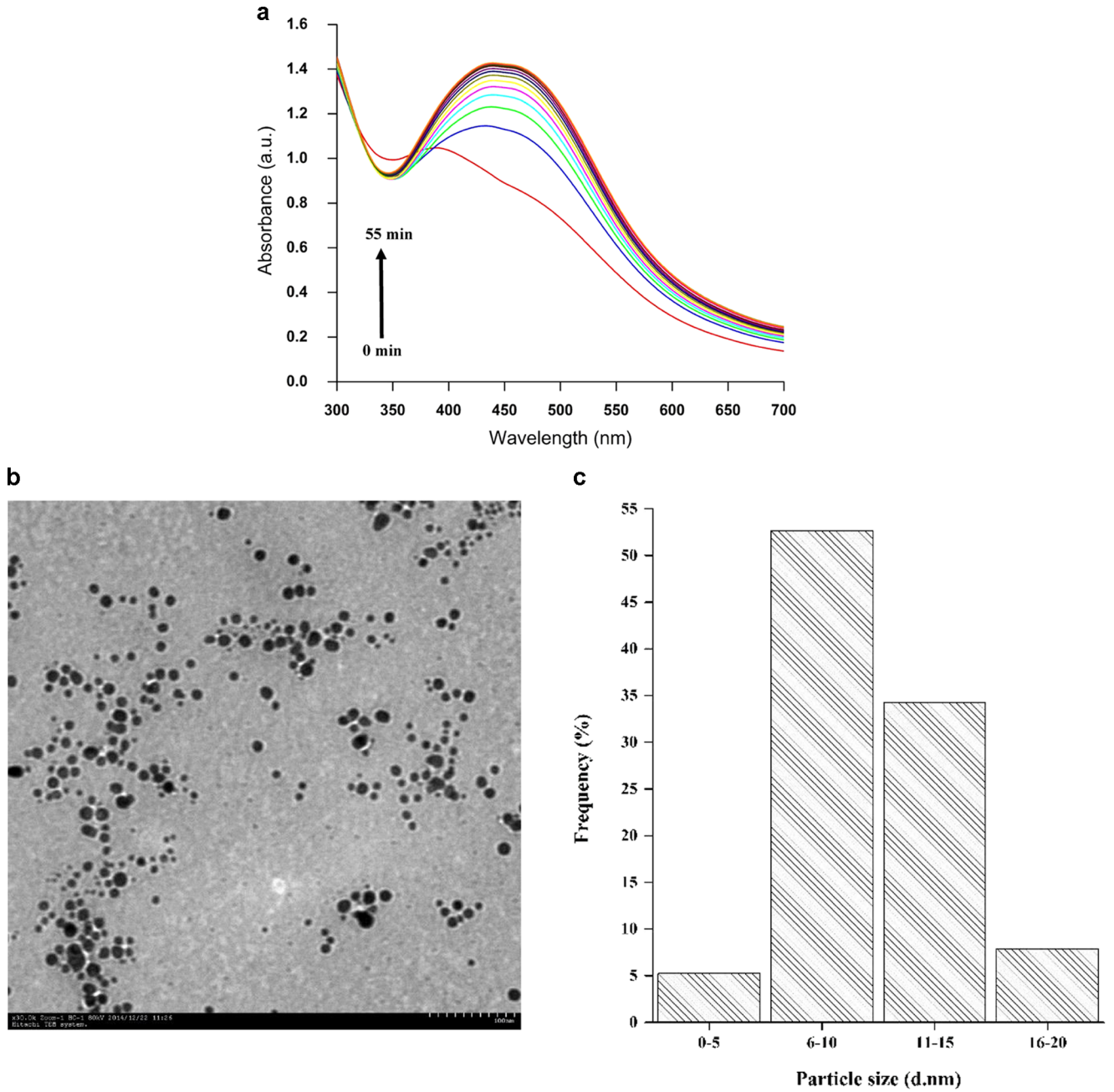

Figure 3. (a) UV−visible spectrum showing gradual synthesis of silver NPs with time. (b) Transmission electron microscopy (TEM) micrographs showing uniformly distributed silver NPs. (c) Particle size distribution histogram of silver NPs as determined using transmission electron micrographs.

ties, nanomaterials have been widely utilized in biomedical applications, among which AgNPs are one of the most promising ones.[23,40−42] In this study, the cytotoxic efficacy of AgNPs was analyzed in two different kinds of human cancer cells: human OS (HOS) and HCC (Huh7) by MTT assay. The cell lines each of mesenchymal origin and epithelial origin were chosen. The AgNPs were selected over free metal silver for exploration of their anticancerous effects because of the enhanced permeability of NPs into tumors, attributable to the EPR effect.[10] Initially, the extracellularly as-synthesized bAgNPs were analyzed for their cytotoxic potential. Interestingly, Huh7 cells were found to be more sensitive (IC_{50}: <5 μg mL^{-1}) to the NPs compared to OS cells (IC_{50}:10 μg mL^{-1}) (Figure 5a). Upon obtaining cytotoxicity with As-*syn*-bAgNPs, silver NPs were separated from the fungal cell-free filtrate by freeze-drying and suspended in water to obtain the bAgNPs, which were used in subsequent experiments. Simultaneously, bare AgNPs were prepared following methods described in Materials and Methods. The cytotoxic potentials of bAgNPs, bare AgNPs, and chemically synthesized AgNPs [cAgNPs, <100 nm, 99.5% metals basis (MKBC1763); Sigma-Aldrich] were compared. The cells were exposed to various concentrations of AgNPs for 24 h and then assessed for their cytotoxicity by the MTT assay. A clear dose-dependent cytotoxicity was observed in the case of protein-capped bAgNPs as compared to that for bare or cAgNPs (Figure 5b,c). Huh7 cells were found to be more sensitive than OS cells to all the tested AgNPs (Figure 5b,c). It can be further inferred that the presence of fungal-derived

DOI: 10.1021/acsomega.7b00045
ACS Omega 2017, 2, 1489−1504

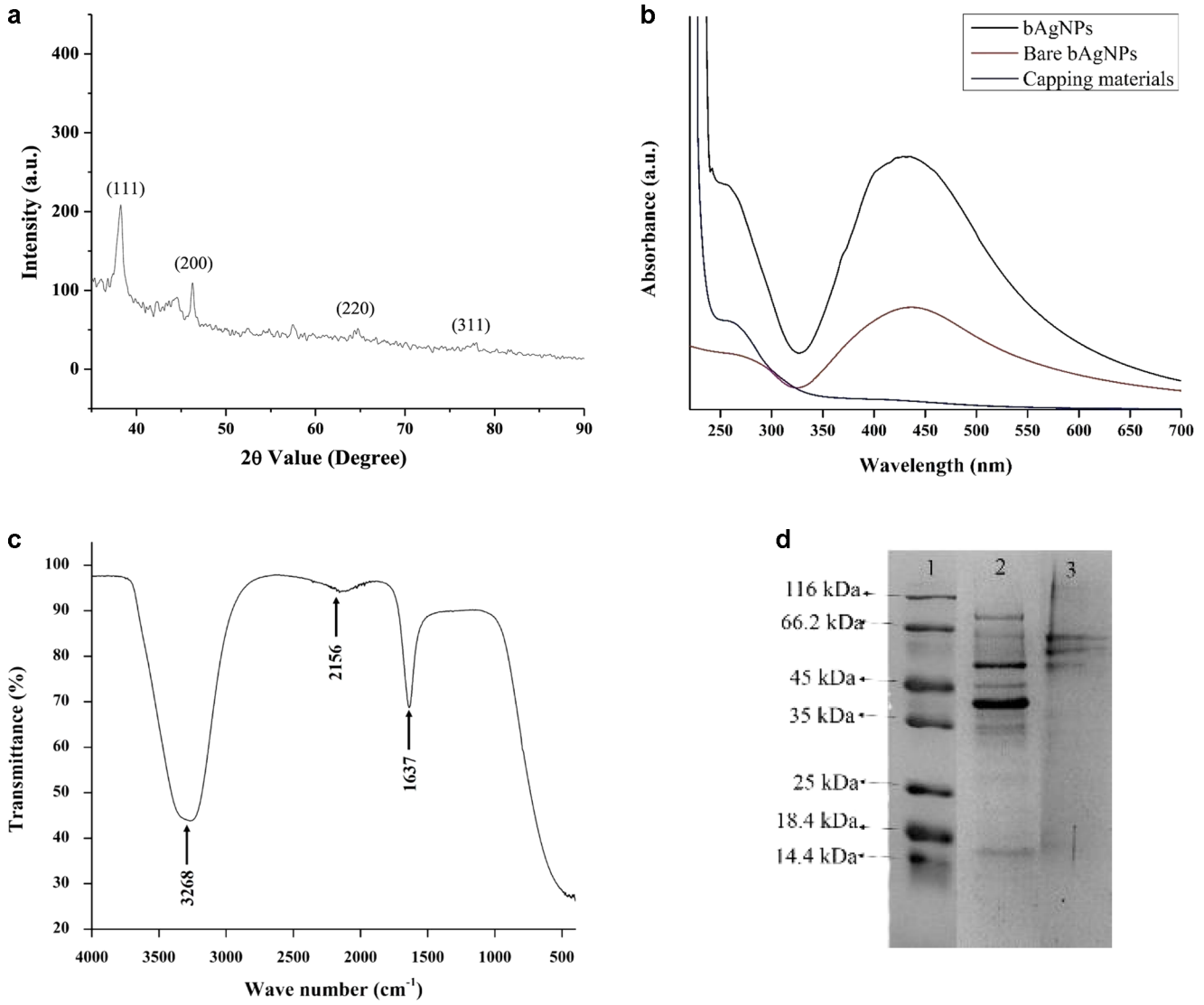

Figure 4. (a) XRD pattern showing crystalline nature of silver NPs. (b) UV−visible absorption spectra showing the presence of proteins (amino acids) in the supernatant, bAgNPs, and their absence in the resuspended NP solution. (c) Fourier transform infrared (FTIR) spectroscopy spectrum of liquid samples showing the presence of proteins on the surface of silver NPs. (d) sodium dodecyl sulfate-polyacrylamide gel electrophoresis (SDS-PAGE) analysis of the purified extracellular proteins of *P. shearii* AJP05. Lane 1, molecular weight marker (SM-0431); lane 2, purified extracellular protein; and lane 3, capping proteins.

components coating and stabilizing bAgNPs probably provide added cytotoxic advantage to them, as bAgNPs were found to be more cytotoxic than bare bAgNPs or cAgNPs. Hence, bAgNPs were subsequently used for further studies.

bAgNPs Enhance Cytotoxicity of Chemotherapeutic Drug Cisplatin (CDDP). Cisplatin, a widely used therapeutic drug is part of the treatment regime for both OS and HCC. However, almost 30 years after the introduction of CDDP into clinical settings, we are still in an effort to understand how to refine the therapeutic potential of cisplatin. Despite its proven benefits, CDDP-based treatment is often associated with life-threatening toxicity, limiting its clinical application.[43] This perpetually demands for identification of novel, biological molecules that can act as a complement to the potent drug CDDP. Keeping these facts in mind, we analyzed whether the protein-capped bAgNPs that showed cytotoxicity against OS and Huh7 cells have prospective potential to increase CDDP-induced cytotoxicity. Our result shows that bAgNPs can efficiently increase the cytotoxic ability of the potent drug, CDDP. The IC_{50} of CDDP was found to be 35 μM in OS cells and 60 μM in Huh7 cells. However, when these cells were exposed to CDDP along with bAgNPs, increased cell cytotoxicity was obtained (Figure 5d,e). This proves that bAgNPs can potentially be used with conventional drugs, such as CDDP, to effectively sensitize both Huh7 and OS cells.

Analysis of bAgNP Internalization. Before investigating the molecular mechanism of cell death upon bAgNP exposure, efforts were made to confirm the internalization of the NPs. The bAgNPs (1) were tagged with the reported luminescent platinum (II) complex.[34] The resulting composite (2) was observed to emit green light under exposure to UV light (λ_{ext} ~ 365 nm) in suspended medium. As the luminescent platinum (II) complex emits green light in water solution, we presumed that the dye has adhered to the surface of NPs (Figure S1a). To support the above proposition, the AgNP−platinum composites were characterized by dynamic light scattering (DLS) (Figure S1b). The measured particle sizes for 1 and 2 were 220 and 249 nm, respectively. The relatively larger size obtained of

DOI: 10.1021/acsomega.7b00045
ACS Omega 2017, 2, 1489−1504

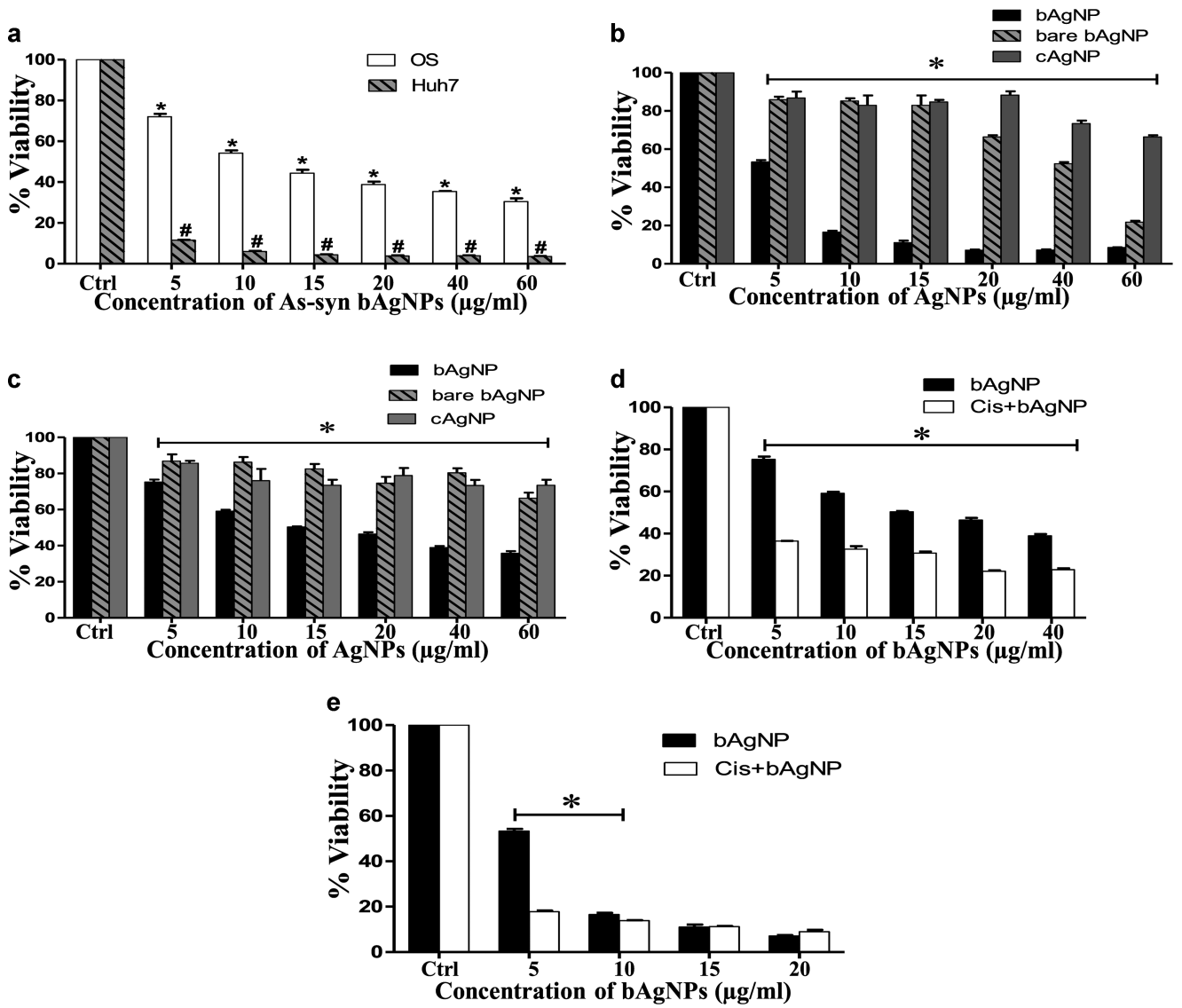

Figure 5. Effect of AgNP treatment on the viability of OS and Huh7 cells. (a) Cells were treated with AgNPs for 24 h, and the cell viability was analyzed through the MTT assay. The cytotoxic effect of As-syn bAgNPs on OS and Huh7 cells is represented through a bar diagram. The symbols (* and #) represent a significant difference ($p < 0.05$) as compared to that in untreated control cells in OS and Huh7 cells, respectively. (b, c) Effect of bAgNP or bare or cAgNP treatment at different concentrations on Huh7 and OS cells, respectively. Here, * represents a significant difference ($p < 0.05$) as compared to that in bare and cAgNP-treated cells. (d, e) Effect of the treatment of a combination of cisplatin (cis) and bAgNP on OS and Huh7 cells, respectively. Here, * represents a significant difference ($p < 0.05$) as compared to that in bAgNP-treated cells.

2 in comparison to that of 1 implies the stacking of the luminescent platinum (II) complex on the surface of 1.[44] Absorption spectra of the luminescent platinum (II) complex and 1 show λ_{max} at 358 and 450 nm, respectively, whereas 2 results both peaks at λ_{max} 358 and 450 nm. Definitely, each peak obtained for 2 is characteristic of the individual components for the luminescent platinum (II) complex and 1, respectively. Interestingly, the characteristic absorption peak for the luminescent platinum (II) complex in 2 is enhanced in comparison to that in bare luminescent platinum (II) complex and the other characteristic surface plasmon band for bAgNP became shallow as compared to the pristine one (Figure S1c). The recorded excitation spectra (Figure S1d) of the luminescent platinum (II) complex and 2 show the maxima at 369 and 398 nm, respectively, but emission spectra (Figure S1d) remain same. On the basis of above observations, we propose that the luminescent platinum (II) complex adheres on the surface of bAgNPs (1). Furthermore, OS cells were treated with the AgNP−Pt(II) complex (2) composite and visualized under a fluorescence microscope. A representative figure of the same demonstrates the presence of green fluorescence inside the cells, indicating efficient internalization of bAgNPs (Figure S2).

AgNP-Induced Cell Cytotoxicity Is ROS-Dependent. Following observances of the cytotoxic potential of bAgNPs, their mechanism of action was investigated. NP-induced ROS generation and oxidative stress have been proposed as mediators of apoptotic cell death previously.[45−47] Furthermore, levels of ROS-scavenging enzymes like peroxidase are also known to be aberrantly regulated in cancer cells.[48,49] However, the ROS inducing potential of the capped-AgNPs is least explored. Hence, the effect of fungal-synthesized AgNPs on intracellular ROS generation was determined in OS and Huh7 cells. The intracellular ROS concentration as measured through

DOI: 10.1021/acsomega.7b00045
ACS Omega 2017, 2, 1489−1504

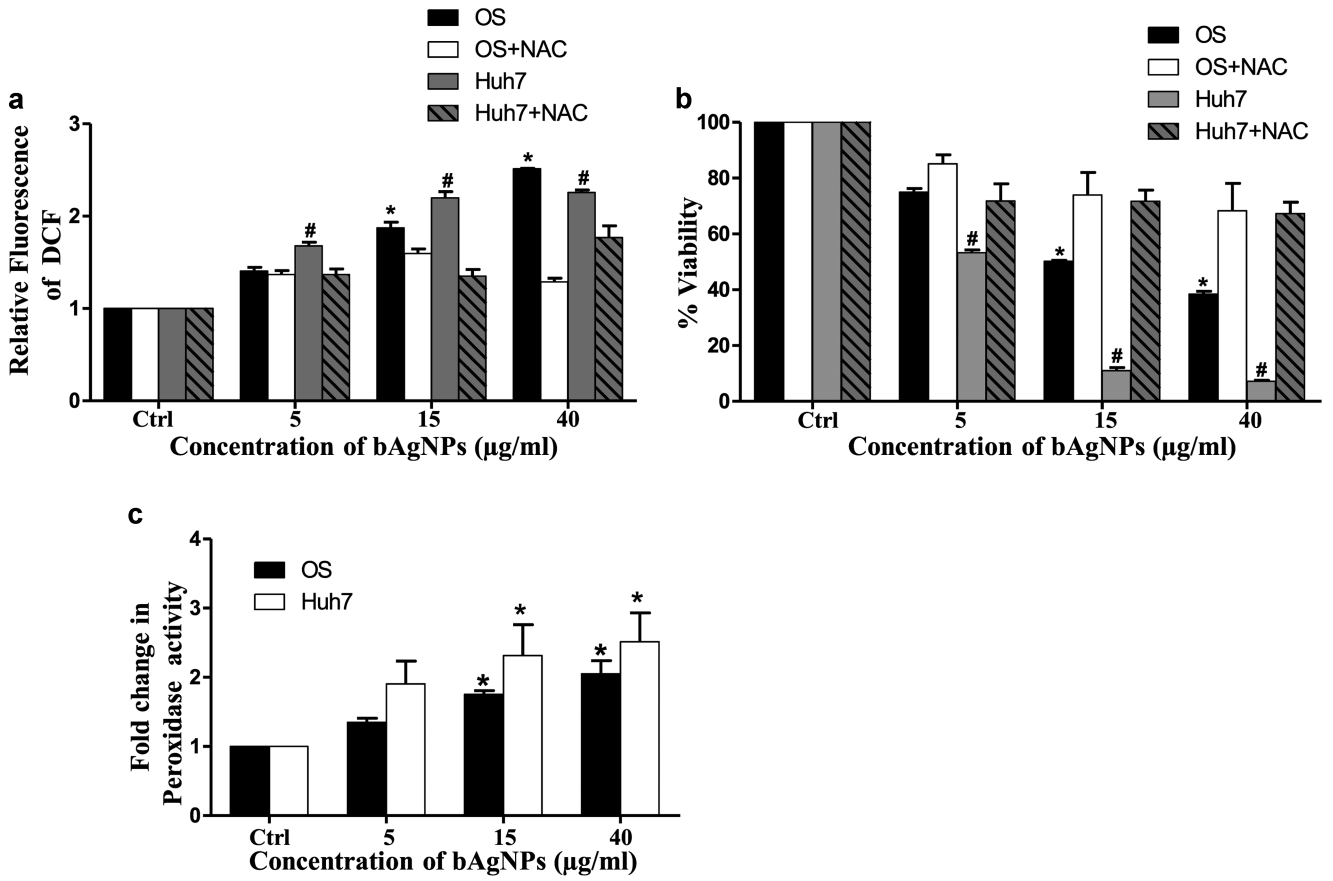

Figure 6. Estimation of ROS levels upon bAgNP treatment. (a) OS and Huh7 cells were exposed to bAgNPs at different concentrations for 24 h. NAC (5 mM) was applied 2 h prior to NP treatment wherever mentioned. Fold change in ROS levels as measured by DCFH-DA is represented with bAgNPs untreated control taken as arbitrary unit "1". (b) MTT assay was performed to check cell viability following exposure of OS and Huh7 cells to bAgNPs with and without NAC (5 mM) treatment. NAC was added 1 h before NP treatment. The * and # symbols represent a statistically significant difference ($p < 0.05$) as compared to that in cells treated with NAC in OS and Huh7 cells, respectively. (c) Fold change in peroxidase enzyme activity with bAgNP treatment in OS and Huh7 cells was measured after 24 h. The untreated control was taken as arbitrary unit "1". The * symbol represents a statistically significant difference ($p < 0.05$) as compared to that in untreated cells.

2,7-dichlorofluorescein diacetate (DCFH-DA) was significantly higher in OS and Huh7 cells treated with bAgNPs (Figure 6a). A decrease in ROS levels was observed when the cells were treated with the widely used ROS scavenger (*N*-acetyl cysteine; NAC) (Figure 6a). Increased ROS production following bAgNP treatment could be one of the reasons for the cytotoxicity of bAgNP in OS and Huh7 cells. To prove the same, we inhibited ROS production by NAC prior to bAgNP treatment and monitored the change in cytotoxicity. Interestingly, ROS inhibition resulted in reduced cytotoxicity in both the cell types but more significantly in Huh7 (Figure 6b). This proved that bAgNP-induced cytotoxicity was ROS-dependent. In addition to ROS, treatment of AgNPs increased the levels of the antioxidant enzyme, peroxidase, in OS and Huh7 cells (Figure 6c). An increased level of antioxidant enzyme might be a compensatory mechanism to cope with high level of oxidative stress due to ROS generated by bAgNP treatment.

Induction of Apoptotic Cell Death by bAgNPs through Activation of Caspases. Morphological variations observed upon bAgNP treatment in both the cell types were captured through bright-field imaging (Figure 7a). Clear indication of rounding up of cells along with some cells showing a stretched phenotype, characteristic of stressed cells, was observed. Furthermore, nuclear staining with 4′-6-diamidino-2-phenylindole (DAPI) showed a fragmented nucleus upon bAgNP exposure (Figure 7b). Morphological alterations provide hints towards the induction of the cell death phenomenon, such as apoptosis, following bAgNP treatment. For further molecular studies, we selected OS cells as they are known to possess inherently resistant characteristics.[50] We investigated the activation of apoptotic markers in OS cells. Caspase-3 has been identified as a major effector of programmed cell death.[49,51] Thus, to investigate the effect of bAgNPs on the apoptotic pathway, the caspase-3 enzyme activity was examined in OS cells through an ELISA-based method. The enzyme activity increased in a dose-dependent manner in bAgNP-treated cells, and an increase of about 1.5 fold was observed at IC_{50} concentration (Figure 7c). An increase in the caspase activity was further confirmed by the detection of cleaved caspase-3, an indicator of apoptosis, by immunoblot (Figure 7d). The cleavage of the poly-ADP-ribose polymerase-1 (PARP-1, 116 kDa) molecule by caspases following DNA damage is also considered as a characteristic marker of apoptosis.[48] Hence, the protein expression of PARP-1 was determined by immunoblot. An increase in the level of cleaved PARP-1 (89 kDa) with simultaneous decrease in total PARP-1 was observed with increasing concentrations of bAgNP exposure (Figure 7e). Furthermore, DNA content analysis with propidium iodide (PI) staining showed an enrichment of fragmented nondiploid cellular DNA and cells representing the

DOI: 10.1021/acsomega.7b00045
ACS Omega 2017, 2, 1489−1504

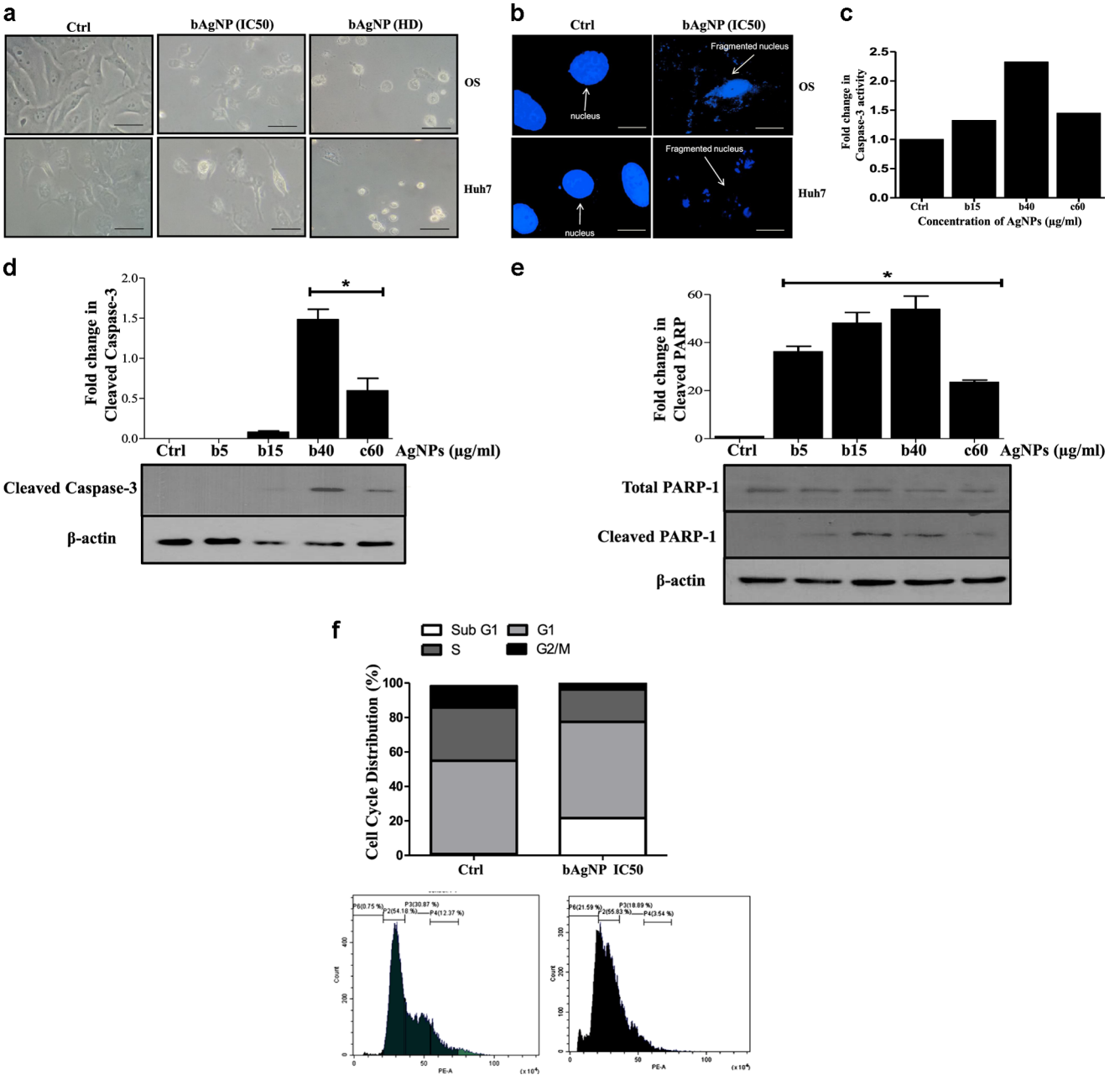

Figure 7. bAgNPs induce apoptosis in OS cells. (a) Phase-contrast images of OS and Huh7 cells after bAgNP treatment (IC_{50} and high dose, i.e., 40 μg mL^{-1} for OS cells and 15 μg mL^{-1} for Huh7 cells) for 24 h. Control (Ctrl) represents untreated cells. The scale bar represents 50 μm. (b) OS and Huh7 cells were seeded on coverslips and treated for 24 h with bAgNPs (IC_{50}). Nuclear fragmentation post-exposure was observed by DAPI staining followed by fluorescence microscopy. The scale bar represents 100 μm. (c) Fold change in the caspase-3 enzyme activity was measured following bAgNP and cAgNP treatment for 24 h. The level of caspase-3 activity in untreated control was taken as arbitrary unit "1". (d, e) Protein levels of cleaved caspase-3, total PARP-1, and cleaved PARP-1 were analyzed by immunoblotting after AgNP exposure in OS cells. β-Actin served as a loading control. Densitometric scanning of blots was performed by ImageJ software and is represented in the bar diagram. [The * symbol represents a significant difference ($p < 0.05$) as compared to that in the control.] (f) Number of cells in each phase of the cell cycle was analyzed by PI staining of OS cells exposed to bAgNPs for 24 h. A representative image of flow cytometric analysis is provided. The percentage of cells in each phase of cell cycle is represented by a bar diagram.

G_1-phase of the cell cycle following bAgNP treatment (Figure 7f). An increase in the number of cells at the subG_1-phase of the cell cycle indicates the presence of apoptotic cells and a probable growth arrest at the G_1/S checkpoint of the cell cycle.[46,52] The above results provide a clear indication toward the induction of DNA damage-mediated apoptotic cascade upon bAgNP treatment.

Autophagy Induction Following bAgNP Treatment Acts as a Survival Strategy. Autophagy is an important intracellular pathway in eukaryotic cells involved in the recycling of cellular materials. It occurs at a basal level in most cells; however, under certain physiological conditions, such as nutrient deprivation, depletion of growth factor, or metabolic stress, autophagy is activated. Activated autophagy can have a dual role depending on the context or cell type; it

DOI: 10.1021/acsomega.7b00045
ACS Omega 2017, 2, 1489−1504

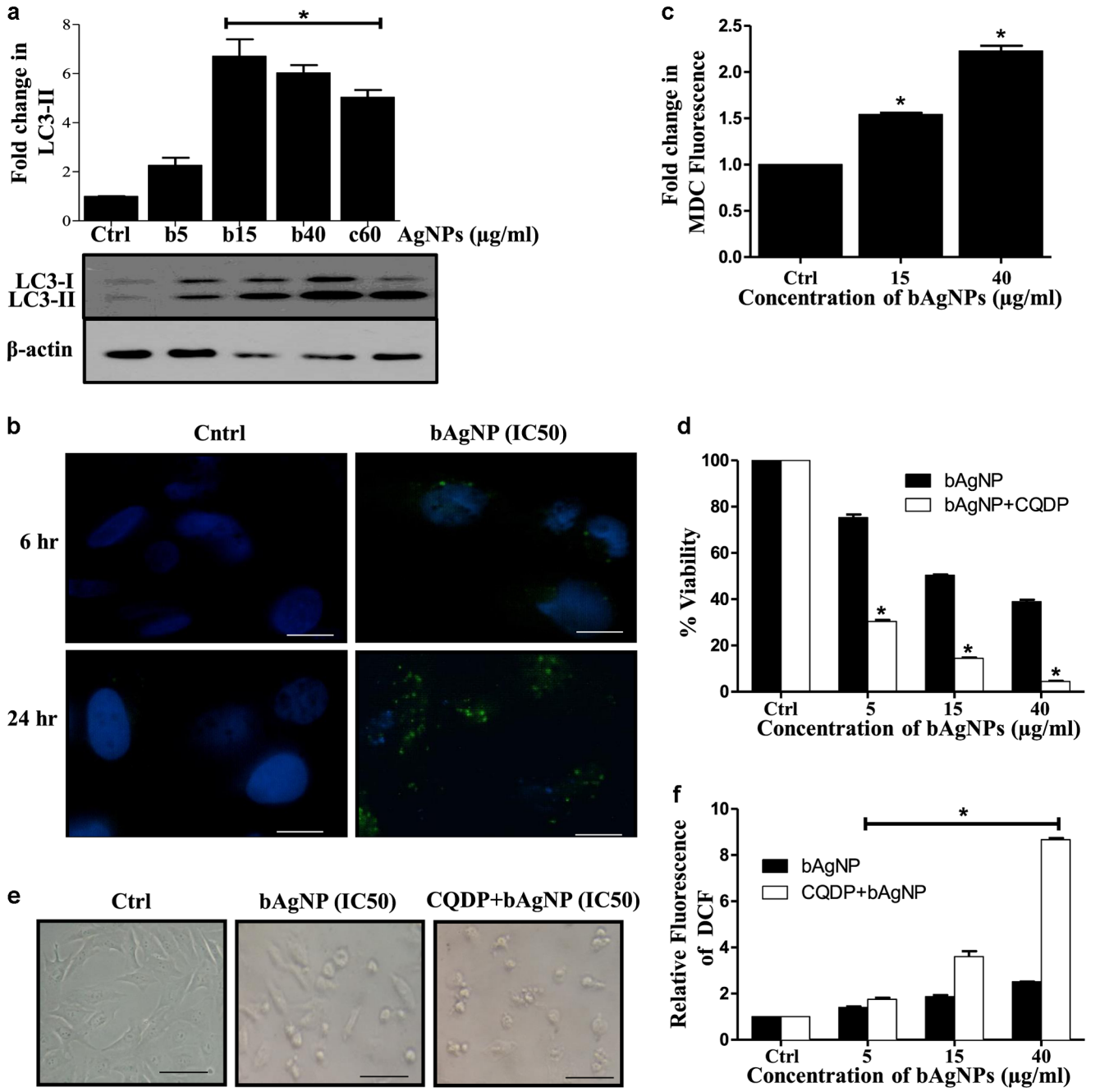

Figure 8. bAgNPs induce autophagy as a survival strategy. (a) Protein expression of autophagy marker LC3B-II was studied by immunoblotting after bAgNP treatment. Densitometric analysis of scanned immunoblots was performed by ImageJ software. β-actin served as a loading control. [The * symbol represents a significant difference ($p < 0.05$) as compared to that in untreated cells.] (b) For further confirmation of autophagy, MDC fluorescence staining was performed after 6 and 24 h of bAgNP treatment in OS cells and green punctate bodies indicative of autophagosomes were monitored by fluorescence microscopy. The scale bar represents 100 μm. (c) Fluorimetric estimation of MDC activity was performed following bAgNP treatment (IC_{50} and high dose, 40 $\mu g\ mL^{-1}$) for 24 h in OS cells. [The * symbol represents a significant difference ($p < 0.05$) as compared to that in untreated cells.] (d) The cytotoxic effect of bAgNPs in OS cells was measured by the MTT assay after 24 h of bAgNP treatment in the presence or absence of the autophagy inhibitor (10 μM CQDP). The inhibitor was added 2 h before the treatment. [The (*) symbol represents a significant difference ($p < 0.05$) as compared to that in bAgNP-treated cells.] (e) Morphological changes observed in OS cells after bAgNP treatment in the presence or absence of the autophagy inhibitor are analyzed by phase contrast microscopy. The scale bar represents 20 μm. (f) ROS levels were measured after autophagy inhibition by CQDP in bAgNP-treated cells by DCFH-DA. ROS levels in untreated cells were taken as arbitrary unit "1". [The * symbol represents a statistically significant difference ($p < 0.05$) as compared to that in only bAgNp treatment.]

can act as a cell-death-inducing mechanism, having crosstalk with apoptotic machinery, or may act as a survival strategy to cope with the cellular stress.[51,53] Therefore, efforts were made to investigate whether autophagy is activated upon bAgNP exposure and its role, if any. The OS cells showed a stark increase in the protein concentration of microtubule-associated protein light chain 3-II (LC3B-II), indicative of the autophagic activity with increasing doses of bAgNPs (Figure 8a). Detection of LC3B-II by immunoblotting is considered as a reliable method for monitoring autophagy. It has been previously

DOI: 10.1021/acsomega.7b00045
ACS Omega 2017, 2, 1489−1504

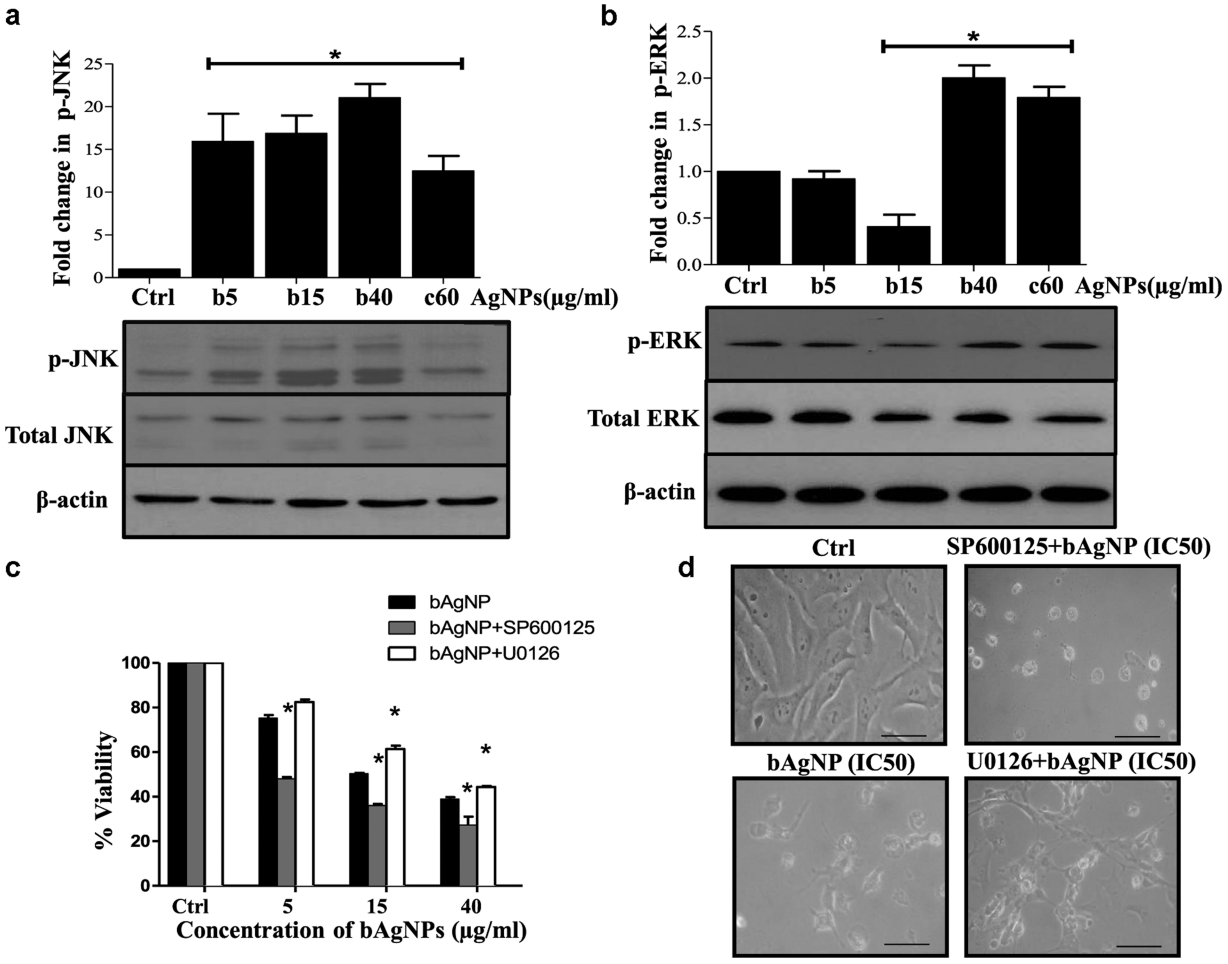

Figure 9. bAgNP causes activation of JNK and ERK signaling in OS cells. (a, b) Protein phosphorylation levels of p-JNK and p-ERK were examined by immunoblotting after bAgNP treatment for 24 h in OS cells. Densitometric analysis of scanned immunoblots was performed by ImageJ software and normalized to β-actin. [The * symbol represents a significant difference ($p < 0.05$) as compared to that in untreated cells.] (c) Cell viability was analyzed by the MTT assay after inhibiting JNK and ERK signaling by SP600125 (25 μM) and U0126 (10 μM), respectively, followed by bAgNP treatment for 24 h. The inhibitors were added 2 h before the NP treatment. [The * symbol represents a statistically significant difference ($p < 0.05$) with respect to the bAgNP treatment.] (d) Morphological changes observed in OS cells after bAgNP treatment in the presence or absence of JNK and ERK inhibitors are analyzed by phase contrast microscopy. The scale bar represents 50 μm.

reported that monodansylcadaverine (MDC) is a specific marker for autolysosomes.[35] We observed the incorporation of MDC in OS cells upon autophagy stimulation by bAgNPs. As depicted in Figure 8b, bAgNP-treated cells showed a stark increase in the number of autophagic vesicles, indicating that bAgNPs induced the formation of MDC-labeled vacuoles. MDC was found to be concentrated as spherical structures or punctate bodies distributed in the cytoplasm of the cells. A fluorimetric measurement of the same provided further evidence for the induction of autophagy upon bAgNP treatment (Figure 8c). Interestingly, prior inhibition of autophagy by the autophagy inhibitor, CQDP, resulted in an increased cell death in OS cells upon bAgNP treatment, suggesting a prosurvival role of autophagy (Figure 8d). Morphological alterations of cells depicting increased cell death upon CQDP and bAgNP treatment are represented in Figure 8e. Furthermore, we observed a stark increase in the levels of ROS post-autophagy inhibition in bAgNP-treated cells (Figure 8f). This indicates that autophagy probably acts as a prosurvival mechanism by suppressing ROS levels upon bAgNP treatment. An inhibition of autophagy, in turn, triggers increased ROS and subsequently more cell death.[54] Therefore, the use of autophagy inhibitor and protein-capped bAgNPs can be an appropriate strategy to treat these cancer cells efficiently. Previously, Jeong et al. reported that autophagy mediated by hypoxia may be a mechanism for resistance to AgNPs-induced apoptosis.[55] However, we report that bAgNPs can itself induce autophagy as a cytoprotective strategy to combat apoptotic cell death. Also, the ability of AgNPs to induce intracellular ROS production is well reported; an elevated ROS is known to exert its effect by lipid, protein, and/or DNA damage, leading to cell death.[49] However, a simultaneous activation of autophagy can limit ROS production through exclusion of damaged mitochondria by mitoautophagy, leading to decreased cell death.[54] In corroboration to above studies, we also observed that an inhibition of autophagy in OS cells elevated bAgNP-induced ROS levels, resulting in enhanced cell death. Here, autophagy thus plays a protective role mainly by preventing enhanced ROS accumulation, probably through the elimination of damaged mitochondria, which are known to be the major generators of ROS.

bAgNP-Induced Activation of Jun N-Terminal Kinase (JNK) and Extracellular Signal-Regulated Kinase (ERK) Mitogen-Activated Protein Kinase (MAPK) Signaling Act

DOI: 10.1021/acsomega.7b00045
ACS Omega 2017, 2, 1489−1504

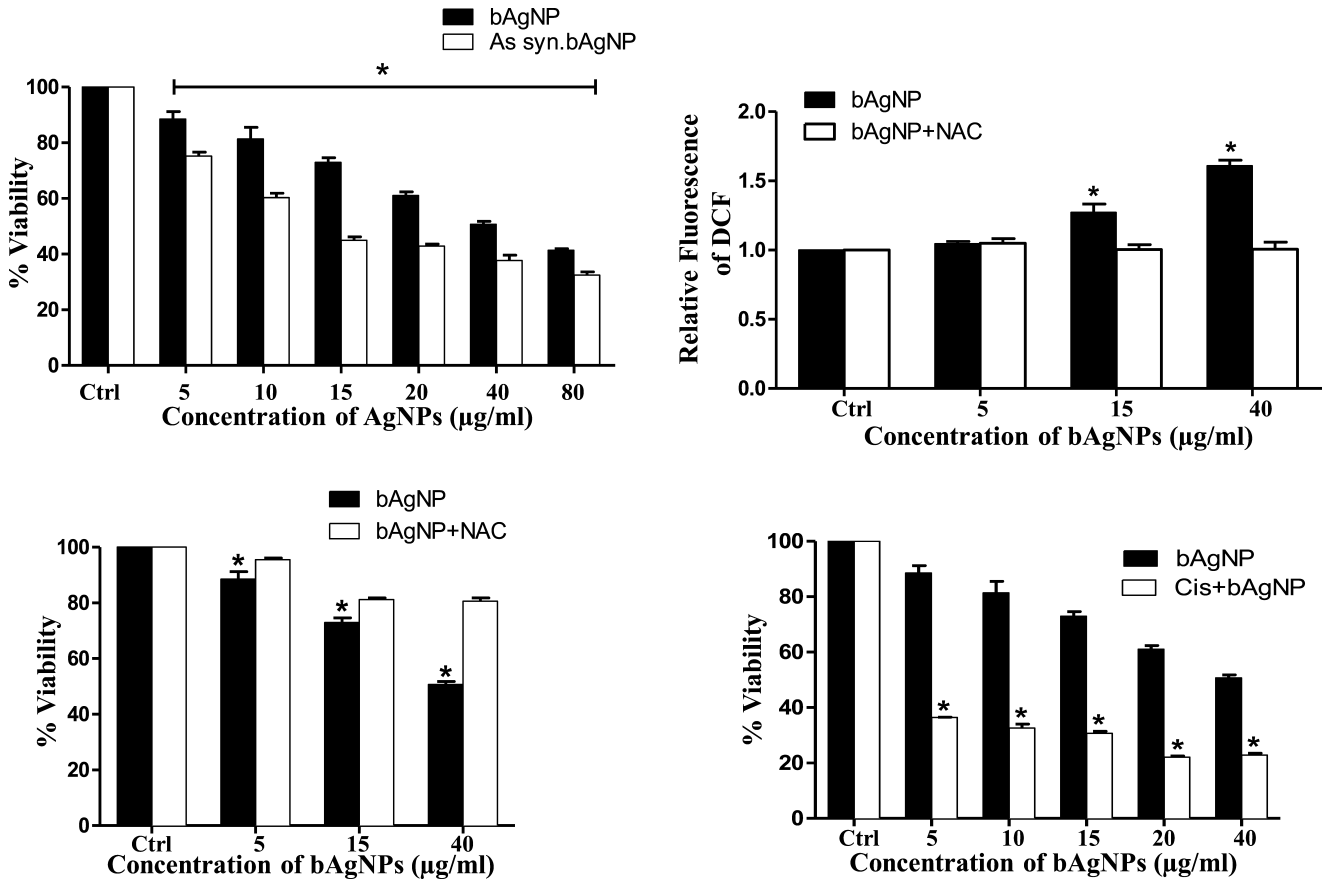

Figure 10. Effect of bAgNPs on the viability of drug-resistant cancer cells. (a) Cell viability was analyzed by the MTT assay after 24 h of bAgNP and As-*syn*-AgNP treatment to resistant OS cells (OS-R). [The * symbol represents a significant difference ($p < 0.05$) as compared to that in untreated cells.] (b) DCFH-DA assay was performed to measure ROS levels in OS-R cells after bAgNP treatment. The cells were exposed to NAC (5 mM) for 1 h before NP treatment. (c) Cell viability after inhibition of ROS by NAC followed by bAgNP treatment for 24 h was measured by the MTT assay. [The * symbol in (b) and (c) represents a statistical significant difference ($p < 0.05$) as compared to that in the cells treated with NAC]. (d) Effect of a combination of cisplatin and bAgNPs on the viability of OS-R cells as measured by the MTT assay after 24 h of exposure. [The (*) symbol represents a significant difference ($p < 0.05$) as compared to that in bAgNP-treated cells.]

Antagonistically. MAPK pathways can regulate several important cellular processes extending from cell survival, metabolism, and differentiation to apoptosis. In this regard, the role of MAPKs, such as ERK and JNK, has been extensively studied in cancer cells; however, their role following AgNP exposure is poorly understood.[47,56,57] The biologically synthesized AgNPs induced the activation of ERK and JNK signaling, as evident by their increased phosphorylation in OS cells after AgNP treatment (Figure 9a,b). More pronounced phosphorylation of ERK and JNK was observed in cells receiving the bAgNP treatment compared to that in cAgNPs (Figure 9a,b). Interestingly, an inhibition of ERK pathway by U0126, a selective inhibitor of the upstream MAP kinases, resulted in decreased cell death after AgNP exposure; however, a pharmacological inhibition of JNK with SP600125 increased the level of AgNP-induced cell death in OS cells, as evaluated by the MTT assay (Figure 9c). Morphological alterations of cells depicting increased cell death upon JNK inhibitor and bAgNP treatment are depicted in Figure 9d. Our results provide strong evidence for selective activation of MAPK pathways following AgNP exposure, where JNK signaling acts as a prosurvival strategy, whereas ERK plays an antagonistic role, inducing prodeath pathways in OS cells. The ultimate cell fate is probably the outcome of disruption of this balance.

bAgNPs Induce Cell Death in Drug-Resistant OS Cells. Acquisition of resistance to chemotherapeutic drugs often hinders the therapy of most cancers, OS is no exception. Therefore, we derived a cisplatin-resistant in vitro model from the parental OS cells and tested for the cytotoxic efficacy of bAgNPs. The OS cells were initially exposed to a high dose of cisplatin followed by clonal selection of surviving cells post-shock, following similar methods described elsewhere. This process was repeated several times to derive OS cells that showed approximately 2-fold decreased sensitivity to cisplatin. These cells are termed as OS-R, representing cells resistant to cisplatin. The concentration of cisplatin at which 50% of OS cells died was 35 μM, whereas an increased viability (80%) was obtained in OS-R at similar concentration of cisplatin. The bAgNPs successfully sensitized the cisplatin-resistant OS cells too; however, as obtained with parental cells, cytotoxicity with as-synthesized NPs was found to be more than that with bAgNPs (Figure 10a). There was an increased production of ROS in OS-R cells too; percentage cytotoxicity of cells decreased with NAC treatment, suggesting a ROS-dependent cell death mechanism (Figure 10b,c). The cytotoxic effects were less pronounced in resistant cells as compared to those in the parental cells. The synergistic effect of cisplatin with bAgNPs was also checked in OS-R similar to what was studied in parental cells. A combination of drugs with NPs was more

DOI: 10.1021/acsomega.7b00045
ACS Omega 2017, 2, 1489−1504

effective in sensitizing the resistant cells too as compared to that of only bAgNPs (Figure 10d). The obtained result provides strong evidence for the potential of bAgNPs in sensitizing both parental and drug-refractory cancer cells.

CONCLUSIONS

The use of biogenic-NPs in therapeutic applications, as an ideal alternative to negate toxicity issues associated with chemically synthesized NPs, is currently an exciting area of research.[40,58] Here, we have synthesized biogenic-AgNPs using a silver-tolerant soil fungal isolate and analyzed their cytotoxic efficacy against aggressive cancer cell types. The protein-capped NPs were found to be way more cytotoxic than bare or chemically synthesized NPs. This might be attributed to the enhanced internalization facilitated by the presence of protein coat or due to controlled release of Ag ions. Further studies characterizing the capping components and their precise function are presently investigated and are excluded from the scope of this study. Detailed investigation of the molecular mechanism leading to cytotoxicity revealed that the mycosynthesized protein-capped bAgNPs induce ROS-dependent apoptosis in OS cells. However, simultaneous induction of autophagy tends to inhibit apoptosis by restricting enhanced ROS production. Furthermore, exploration of the signaling pathway revealed that JNK activation acts as a prosurvival response whereas ERK a proapoptotic one, upon AgNp exposure in OS cells. Furthermore, the protein-capped bAgNPs were found to enhance the cytotoxicity of the widely used chemotherapeutic agent, like CDDP, and also were able to effectively sensitize drug-resistant cells. To the best of our knowledge, this is the first study with biologically synthesized AgNPs from *P. shearii* isolate AJP05, which not only describes the cytotoxic potential of the protein-capped bAgNPs but also holistically characterizes the molecular signaling involved. The implications from this study can be exploited for future potential therapeutic benefits against aggressive-type cancers given that NPs have this unique ability to home specifically into tumor tissues by utilizing their leaky vasculature by the EPR effect.

MATERIALS AND METHODS

Materials. All chemicals (analytical grade) used in the present study were procured from Sigma-Aldrich or Merck unless otherwise stated. The culture media were obtained from HiMedia and Invitrogen. Protein molecular weight marker (SM-0431) was purchased from MBI Fermentas.

Metal Tolerance Profile and Screening of Fungal Isolates. A maximum tolerable concentration (MTC) assay was performed to determine the silver metal tolerance ability of fungi isolated from metal-rich rhizospheric soil. The complete details of isolation and molecular characterization of fungal isolates can be obtained from our recent report.[31] To determine the silver metal tolerance ability, experimental plates were prepared by supplementing Czapek dox agar medium (pH 7.3) with varying amounts of silver nitrate ($AgNO_3$) to obtain a final concentrations of silver ions in the ranges of 250, 500, 750, 1000, 1250, 1500, and 2000 $\mu g\ mL^{-1}$. Plates without silver ions were used as control. Each plate was inoculated with the test fungal isolate (10^6 cfu mL^{-1}) followed by incubation for 4 days at 28 °C under dark conditions. The experiment was performed in triplicate. The maximum concentration of silver ions that allowed the growth of a fungus in all three replicates was considered as the MTC. All the fungal isolates were screened to check their ability for extracellular synthesis of silver NPs based on the visual inspection and UV−visible spectroscopic analysis. The fungal isolate showing significant metal tolerance as well as quick and efficient extracellular synthesis of AgNPs was chosen for further studies.

Extracellular Synthesis of Silver NPs. The protocol followed for extracellular synthesis of silver NPs was adopted from our previous report.[26] Briefly, the selected fungal isolate was fermented in 80 mL of MGYP medium (0.3% malt extract, 1.0% glucose, 0.3% yeast extract, 0.5% peptone; pH 7.0) at 28 °C for 72 h on a rotary shaker (150 rpm) under dark conditions. The fungal biomass was separated by centrifugation (8000 rpm, 10 min, and 4 °C) and washed thrice using sterile distilled water to remove all traces of culture media. Biomass (10 g; fresh weight) was resuspended in 50 mL of sterile double-distilled water and further incubated for 72 h under similar conditions as described above. The fungal cell-free filtrate containing extracellular metabolites was collected by separating the biomass by vacuum filtration. Aqueous silver nitrate solution was added to the flasks containing 100 mL of fungal cell-free filtrate at a final concentration of 1.0 mM and incubated until the color of the solution changed to brown under the similar conditions as described above. Controls containing the fungal cell-free filtrate (without silver nitrate) and pure silver nitrate solution (without fungal cell-free filtrate) were also incubated simultaneously along with experimental flasks in three replicates.

Preparation of Bare bAgNPs. The protocol for the preparation of bare bAgNPs was adopted from our previous report[18] with minor modifications as detailed below. All the steps including centrifugation (12 000 rpm; 30 min) were carried out at 4 °C. The as-synthesized protein-capped silver NP solution was centrifuged, and the pellet was washed thrice with water, keeping intermittent vortexing and centrifugation to remove unbounded protein molecules. The obtained pellet was suspended in 1% (w/v) SDS and boiled in a water bath for 15 min followed by centrifugation. SDS is a widely used denaturing agent, and its treatment results in the detachment of the surface-bounded proteins from NPs.[18] The supernatant containing the unreacted SDS and SDS−protein complex was analyzed for the presence of proteins by measuring the UV−visible absorption spectrum. The resulting pellet was boiled in 1 mL of Tris-Cl (pH 8.0) in a water bath for 10 min to eliminate the possibility of SDS binding to the NPs, if any. To ensure the complete removal of SDS, dialysis was carried out against milli-Q water with four changes followed by centrifugation. The obtained bare silver NPs were characterized using UV−visible spectroscopy measurement.

Characterization of NPs. *Visual Observation.* The color change of the cell-free filtrate from pale yellow to brown after addition of silver nitrate was routinely monitored visually, which would signify the bioreduction of silver ions and formation of AgNPs.

UV−Visible Spectroscopy. The gradual synthesis of AgNPs was monitored using UV−visible spectroscopy by sampling of aliquots (1 mL) at different time intervals. The absorption spectra were measured on a Jasco V-630 UV−visible spectrophotometer (Jasco Corporation, Japan) operated within the range of 200−700 nm at a resolution of 1 nm.

TEM. Samples for TEM were prepared by drop-coating the as-synthesized NP solution onto carbon-coated copper grids. The extra solution was removed using a lint-free blotting paper after a minute, and the grids were kept in a vacuum desiccator

DOI: 10.1021/acsomega.7b00045
ACS Omega 2017, 2, 1489−1504

overnight. TEM micrographs were taken on a Hitachi H-7650 TEM instrument (Hitachi High-Technologies Corporation, Japan) at an acceleration voltage of 100 kV.

XRD. XRD measurements of the freeze-dried samples were carried out using a Rigaku MiniFlex II Bench top XRD System (Rigaku Company) operated at a voltage of 20 kV and current of 15 mA with Cu Kα radiation. The crystal phase was analyzed by comparing the calculated values of interplanar spacing and the corresponding intensities of diffraction peaks with the standard theoretical values of the Powder Diffraction File database (PCPDFWIN; JCPDS-ICDD 2008).

Characterization of Capping Molecules. *FTIR Spectroscopy.* The freeze-dried as-synthesized NPs were mixed with potassium bromide in a ratio of 1:100, and the FTIR analysis was performed on a Perkin Elmer Frontier FTIR spectrometer (Perkin Elmer) in the range of 400−4000 cm^{-1} at a resolution of 4 cm^{-1}.

SDS-PAGE. To investigate the proteins present on the surface of bAgNPs, the as-synthesized NPs were boiled with 1% SDS solution for 15 min followed by centrifugation at 120 00 rpm for 30 min to collect the capping proteins in the supernatant. SDS-PAGE was carried out to determine the molecular weight of capping molecules as described by Laemmli, 1970.[32] The sample containing capping proteins was mixed in a 1:1 ratio with the Laemmli sample buffer [0.5 M Tris−HCl (pH 6.8), 0.5% bromophenol blue, 10% glycerol, 5% β-mercaptoethanol, and 2% SDS] and incubated for 5 min at 100 °C in a boiling water bath. The preparations were centrifuged (12 000 rpm, 5 min, and 4 °C), and the supernatant was used for electrophoresis on a Mini Protean gel system (Bio-Rad) at a constant voltage of 120 V at room temperature. After electrophoresis, the gel was stained with 0.25% Coomassie brilliant blue (CBB) R-250 in the 45% methanol−10% acetic acid solution for 3 h followed by overnight destaining in the 45% methanol−10% acetic acid solution. The molecular mass of the protein bands was determined by interpolation from a semilogarithmic plot of relative molecular mass versus the R_f value (relative mobility).

Cell Culture and Pharmacological Inhibitors. Human cancer cell lines, HOS CRL-1543 (OS) (obtained from NCCS, Pune, India) and Huh7 (kind gift from Dr. Soma Banerjee), were cultured at 37 °C, 5% CO_2, in minimum essential medium (MEM; HiMedia) and Dulbecco's modified eagle medium (DMEM; Invitrogen) supplemented with 10% fetal bovine serum (FBS; Invitrogen), respectively. Penicillin (100 U mL^{-1}) and streptomycin (100 μg mL^{-1}; Invitrogen) were added to the culture medium. The cells were typically grown to 60−70% confluency, rinsed in phosphate-buffered saline (PBS; Invitrogen), and placed into fresh medium prior to treatments. Primary and secondary antibodies used for immunoblotting, the MEK inhibitor (U0126), and the autophagy inhibitor (chloroquine diphosphate, CQDP) were purchased from Cell Signaling Technology. The JNK inhibitor (SP600125) was purchased from Santa Cruz Biotechnology. The ROS scavenger, NAC, was procured from SRL.

In Vitro Cytotoxicity Assay. In vitro cytotoxicity assay was performed as described previously by Chowdhury et al.[33] Briefly, the cells were cultured in 96-well plates. After 24 h, the cells were treated with drugs or NPs or compounds for specific period of time. Thereafter, MTT (3-(4,5-dimethylthiazol-2-yl)-2,5-diphenyltetrazolium bromide) (SRL) was added to each treated and control well and the cells were incubated for 4 h. Formazan crystals were solubilized in dimethyl sulfoxide (DMSO), and readings were obtained at 570 nm with a differential filter of 630 nm using a multiskan microplate spectrophotometer (Thermo Scientific). The percentage of viable cells was calculated using the following formula: viability (%) = (mean absorbance value of drug-treated cells)/(mean absorbance value of control) × 100. A concentration of 0.2% DMSO was found to be nontoxic and was used for dissolving CDDP and used as a control in cytotoxicity experiments.

Microscopic Imaging and NP Internalization. For bright-field microscopic imaging, the cells were cultured at a desired density in 6 cm culture dishes, treated with AgNPs, and then images were captured using Olympus (CKX41) microscope at 20× magnification. For detection of nuclear fragmentation, the cells were grown overnight on coverslips in 6 cm culture dishes and were treated with AgNPs for 24 h. Coverslip-cultured cells were washed with 0.1 M PBS and fixed in methanol at −20 °C for 10 min. The coverslips were mounted with an antifade mountant containing DAPI (Thermo Scientific) on a glass slide. Nuclear morphology was observed by fluorescence microscopy (Olympus, BX41). For the analysis of internalization of AgNPs, we prepared AgNP-luminescent platinum (II) composites. Briefly, 3 mg of the luminescent platinum (II) complex was added into a suspension of 10 mg of bAgNPs taken in distilled H_2O (2 mL). It was stirred overnight at room temperature. Then, the reaction mixture was filtered with 55 mm Whatman qualitative filter paper #2 and the filtrate was characterized using DLS on a Malvern Zetasizer Nano-ZS spectrometer (Malvern Instruments, U.K.). Measurements were recorded at 25 °C ± 1 °C, in triplicates; each measurement was the average of 20 data sets acquired for 10 s each.[34] Thereafter, following confirmation of composite formation, AgNP internalization was confirmed by the exposure of platinum−AgNP composite on OS cells for 1 h and its subsequent visualization by a fluorescence microscope using FITC ($\lambda_{ex/em}$ 490/520) and DAPI ($\lambda_{ex/em}$ 372/456) filters.

Staining with MDC. Drug MDC, a specific autophagolysosomal marker, was used to analyze the autophagic process. For visualization of autophagic vacuoles by microscopy, OS cells were plated on coverslips overnight. Following bAgNP treatment, the cells were incubated for 10 min with 0.05 mM MDC in PBS at 37 °C.[35] After incubation, the coverslips containing the cells were washed with PBS and mounted with the antifade mountant (containing DAPI). Intracellular MDC in the form of punctate dots were analyzed by fluorescence microscopy. For fluorimetric measurement, after incubation of cells with bAgNP and labeling with MDC for 10 min, the cells were washed with PBS and collected in 10 mM Tris−HCl (pH 8) containing 0.1% TritonX-100. Intracellular MDC was measured by fluorescence photometry (excitation 380 nm and emission 525 nm) in a microplate reader (Fluoroskan Ascent).[36] An increase in MDC fluorescence upon bAgNP treatment was expressed as a fold change with respect to control.

Measurement of Intracellular ROS and Antioxidant Enzyme Activity. ROS levels were estimated using DCFH-DA (Sigma), which measures intracellular generation of hydrogen peroxide, a procedure for estimating ROS. DCFH-DA passively enters the cell, where it reacts with ROS to form the highly fluorescent compound, dichlorofluorescein (DCF). Approximately, 0.3 × 10^4 cells were seeded and treated with AgNPs at different concentrations for 24 h and 5 mM NAC was added 2 h prior AgNP treatment wherever mentioned to inhibit ROS. Following exposure to AgNPs, the cells were washed with

DOI: 10.1021/acsomega.7b00045
ACS Omega 2017, 2, 1489−1504

PBS and then incubated in 100 μL of working solution of DCFH-DA (2 mM DCFH-DA stock solution was diluted to yield a 20 μM working solution) at 37 °C for 30 min. The fluorescence was measured at 485 nm excitation and 530 nm emission using a microplate reader (Fluoroskan Ascent).[37]

To measure peroxidase enzyme activity,[18] 0.05 M pyrogallol was added to 100 μL of the protein lysate. The reaction was started by adding 1% H_2O_2. Change in absorbance after every 30 s interval for 3 min was observed in Multiskan Microplate Spectrophotometer at 420 nm. The enzyme activity was measured as a change in absorbance/min/mg of protein. Pyragallol in the presence of H_2O_2 is oxidized to purpurogallin, a colored derivative, by the peroxidase enzyme. The values were expressed as a fold change with respect to control.

Caspase Assay. The cells (1×10^4/well) were seeded and exposed to different concentrations of AgNPs for 24 h. The activity of caspase-3 was measured using the caspase-3 colorimetric protease assay kit (Invitrogen) following the manufacturer's protocol. Briefly, the cell lysate was collected in RIPA buffer, and the concentration of protein was determined using the Bradford assay. Equal amount (60 μg) of protein mixed with the reaction buffer was added to microtiter plates following incubation with the caspase-3 substrate (acetyl-Asp-Glu-Val-Asp *p*-nitroanilide, Ac-DEVD-pNA) for 1 h, and the absorbance was read at 405 nm using a microplate reader (Start-fax 2100, Awareness Tech. Ltd). The colorimetric assay is based on the hydrolysis of the caspase-3 substrate by the caspase-3 enzyme, resulting in the release of the *p*-nitroaniline (pNA) moiety. The concentration of the pNA released from the substrate was calculated from the absorbance values at 405 nm.

Cell Cycle Analysis. For the detection of cells at different phases of the cell cycle, they were seeded at a density of 1×10^6, grown overnight, and exposed to bAgNPs for 24 h. Following incubation, the cells were harvested and fixed in 70% ethanol for 24 h at −20 °C. Thereafter, the cells were centrifuged at 1500 rpm and the cell pellet obtained was resuspended in PBS. Then, PI (20 μg mL^{-1}) was added and the dye-added mixture was incubated in dark for 30 min before events were acquired in a flow cytometer (CytoFLEX, Beckman Coulter).[33] The percentage of cells in each phase of cell cycle was calculated and plotted in a bar diagram.

Immunoblotting. Immunoblotting was performed as described previously.[33] The cells were lysed in a modified RIPA buffer (Sigma-Aldrich), and the protein content was measured using the Bradford reagent. Then, the loading buffer was added to the lysates followed by heat denaturation (100 °C for 10 min) and cooling on ice. Equal concentrations of protein lysates were loaded in denaturing polyacrylamide gels and thereafter transferred to the PVDF membrane (Millipore) for blocking with 5% skimmed milk (HiMedia). The blots were probed with a specific primary antibody (dilution 1:1000). β-Actin (Santa Cruz Biotechnology; dilution 1:2000) was used as a loading control. The secondary antibodies used were horseradish peroxide-conjugated goat antirabbit IgG. The protein intensity was detected using the enhanced chemiluminescence detection system (Thermo Scientific). The expression was densitometrically quantified using ImageJ software and normalized to control.

Creation of Drug-Resistant Cell Line. The OS cell line resistant to cisplatin (CDDP; OS-R) was created following similar methods described before.[38] Briefly, OS cells were exposed to repeated doses of very high concentration of CDDP (1 mg mL^{-1}); the surviving cells were selected and further subcultured. OS-R cells were periodically checked for their resistance property by the MTT assay.

Statistical Analysis. The obtained data were analyzed using the Prism software (Version 5.01; GraphPad Software Inc.). The effect of various treatments was statistically analyzed using one-way ANOVA or Student's *t*-test, and the level of $p < 0.05$ was considered as statistically significant. All data points represent the mean of independent measurements. Uncertainties were represented as standard deviations in the form of bars.

■ ASSOCIATED CONTENT

Supporting Information

The Supporting Information is available free of charge on the ACS Publications website at DOI: 10.1021/acsomega.7b00045.

Representation of luminescent platinum (II) complex on bAgNPs (Figure S1a); particle size distribution obtained by DLS (Figure S1b); absorption spectra for luminescent platinum (II) complex (Figure S1c); excitation and emission spectra for luminescent platinum (II) complex and bAgNP-Pt(II) complex composite (Figure S1d); internalization of bAgNPs (Figure S2) (PDF)

■ AUTHOR INFORMATION

Corresponding Authors

*E-mail: rajdeep.chowdhury@pilani.bits-pilani.ac.in. Tel: +91 1596 515608. Fax: +91 1596 244183 (R.C.).

*E-mail: drjitendrapanwar@yahoo.co.in. Tel: +91 1596 515728, Fax: +91 1596 244183 (J.P.).

ORCID

Jitendra Panwar: 0000-0002-0750-9745

Author Contributions

§L.F. and V.P. contribute equally to this work.

Notes

The authors declare no competing financial interest.

■ ACKNOWLEDGMENTS

This research work was financially supported by the Department of Science and Technology, Government of India, New Delhi, under the SERB (SB/FT/LS-233/2012) and Nano Mission Scheme (SR/NM/NS-1132/2011). The authors are grateful to the Advanced Instrumentation Research Facility, Jawaharlal Nehru University, New Delhi, India, for TEM and XRD analyses and Birla Institute of Technology and Science, Pilani, for providing lab facilities. L.F. thanks UGC-CSIR, Government of India, for providing research scholarship.

■ REFERENCES

(1) Heiligtag, F. J.; Niederberger, M. The fascinating world of nanoparticle research. *Mater. Today* **2013**, *16*, 262−271.

(2) Parak, W. J.; Nel, A. E.; Weiss, P. S. Grand challenges for nanoscience and nanotechnology. *ACS Nano* **2015**, *9*, 6637−6640.

(3) Asharani, P.; Hande, M. P.; Valiyaveettil, S. Anti-proliferative activity of silver nanoparticles. *BMC Cell Biol.* **2009**, *10*, 65.

(4) Austin, L. A.; Mackey, M. A.; Dreaden, E. C.; El-Sayed, M. A. The optical, photothermal, and facile surface chemical properties of gold and silver nanoparticles in biodiagnostics, therapy, and drug delivery. *Arch. Toxicol.* **2014**, *88*, 1391−1417.

(5) He, Y.; Du, Z.; Ma, S.; Liu, Y.; Li, D.; Huang, H.; Jiang, S.; Cheng, S.; Wu, W.; Zhang, K. Effects of green-synthesized silver nanoparticles on lung cancer cells in vitro and grown as xenograft tumors in vivo. *Int. J. Nanomed.* **2016**, *11*, 1879−1887.

DOI: 10.1021/acsomega.7b00045
ACS Omega 2017, 2, 1489−1504

(6) Roco, M. C. International perspective on government nanotechnology funding in 2005. *J. Nanopart. Res.* **2005**, *7*, 707−712.
(7) Marambio-Jones, C.; Hoek, E. M. A review of the antibacterial effects of silver nanomaterials and potential implications for human health and the environment. *J. Nanopart. Res.* **2010**, *12*, 1531−1551.
(8) Prabhu, S.; Poulose, E. K. Silver nanoparticles: mechanism of antimicrobial action, synthesis, medical applications, and toxicity effects. *Int. Nano Lett.* **2012**, *2*, 32.
(9) Holohan, C.; Van Schaeybroeck, S.; Longley, D. B.; Johnston, P. G. Cancer drug resistance: an evolving paradigm. *Nat. Rev. Cancer* **2013**, *13*, 714−726.
(10) Prabhakar, U.; Maeda, H.; Jain, R. K.; Sevick-Muraca, E. M.; Zamboni, W.; Farokhzad, O. C.; Barry, S. T.; Gabizon, A.; Grodzinski, P.; Blakey, D. C. Challenges and key considerations of the enhanced permeability and retention effect for nanomedicine drug delivery in oncology. *Cancer Res.* **2013**, *73*, 2412−2417.
(11) Ong, C.; Lim, J.; Ng, C.; Li, J.; Yung, L.; Bay, B. Silver nanoparticles in cancer: therapeutic efficacy and toxicity. *Curr. Med. Chem.* **2013**, *20*, 772−781.
(12) Locatelli, E.; Naddaka, M.; Uboldi, C.; Loudos, G.; Fragogeorgi, E.; Molinari, V.; Pucci, A.; Tsotakos, T.; Psimadas, D.; Ponti, J. Targeted delivery of silver nanoparticles and alisertib: in vitro and in vivo synergistic effect against glioblastoma. *Nanomedicine* **2014**, *9*, 839−849.
(13) Sanpui, P.; Chattopadhyay, A.; Ghosh, S. S. Induction of apoptosis in cancer cells at low silver nanoparticle concentrations using chitosan nanocarrier. *ACS Appl. Mater. Interfaces* **2011**, *3*, 218−228.
(14) Gengan, R. M.; Anand, K.; Phulukdaree, A.; Chuturgoon, A. A549 lung cell line activity of biosynthesized silver nanoparticles using Albizia adianthifolia leaf. *Colloids Surf., B* **2013**, *105*, 87−91.
(15) Jeyaraj, M.; Sathishkumar, G.; Sivanandhan, G.; MubarakAli, D.; Rajesh, M.; Arun, R.; Kapildev, G.; Manickavasagam, M.; Thajuddin, N.; Premkumar, K. Biogenic silver nanoparticles for cancer treatment: an experimental report. *Colloids Surf., B* **2013**, *106*, 86−92.
(16) Jeyaraj, M.; Rajesh, M.; Arun, R.; MubarakAli, D.; Sathishkumar, G.; Sivanandhan, G.; Dev, G. K.; Manickavasagam, M.; Premkumar, K.; Thajuddin, N. An investigation on the cytotoxicity and caspase-mediated apoptotic effect of biologically synthesized silver nanoparticles using *Podophyllum hexandrum* on human cervical carcinoma cells. *Colloids Surf., B* **2013**, *102*, 708−717.
(17) Xiu, Z.-m.; Zhang, Q.-b.; Puppala, H. L.; Colvin, V. L.; Alvarez, P. J. Negligible particle-specific antibacterial activity of silver nanoparticles. *Nano Lett.* **2012**, *12*, 4271−4275.
(18) Jain, N.; Bhargava, A.; Rathi, M.; Dilip, R. V.; Panwar, J. Removal of Protein Capping Enhances the Antibacterial Efficiency of Biosynthesized Silver Nanoparticles. *PLoS One* **2015**, *10*, No. e0134337.
(19) Harper, S.; Usenko, C.; Hutchison, J.; Maddux, B.; Tanguay, R. In vivo biodistribution and toxicity depends on nanomaterial composition, size, surface functionalisation and route of exposure. *J. Exp. Nanosci.* **2008**, *3*, 195−206.
(20) Kennedy, D. C.; Orts-Gil, G.; Lai, C.-H.; Müller, L.; Haase, A.; Luch, A.; Seeberger, P. H. Carbohydrate functionalization of silver nanoparticles modulates cytotoxicity and cellular uptake. *J. Nanobiotechnol.* **2014**, *12*, 59.
(21) Yoo, K.-C.; Yoon, C.-H.; Kwon, D.; Hyun, K.-H.; Woo, S. J.; Kim, R.-K.; Lim, E.-J.; Suh, Y.; Kim, M.-J.; Yoon, T. H. Titanium dioxide induces apoptotic cell death through reactive oxygen species-mediated Fas upregulation and Bax activation. *Int. J. Nanomed.* **2012**, *7*, 1203−1214.
(22) Jain, N.; Bhargava, A.; Majumdar, S.; Tarafdar, J.; Panwar, J. Extracellular biosynthesis and characterization of silver nanoparticles using *Aspergillus flavus* NJP08: a mechanism perspective. *Nanoscale* **2011**, *3*, 635−641.
(23) Thakkar, K. N.; Mhatre, S. S.; Parikh, R. Y. Biological synthesis of metallic nanoparticles. *Nanomedicine* **2010**, *6*, 257−262.
(24) Bhargava, A.; Jain, N.; Barathi, M.; Akhtar, M. S.; Yun, Y.-S.; Panwar, J. Synthesis, characterization and mechanistic insights of mycogenic iron oxide nanoparticles. *J. Nanopart. Res.* **2013**, *15*, 2031.
(25) Durán, N.; Marcato, P. D.; Durán, M.; Yadav, A.; Gade, A.; Rai, M. Mechanistic aspects in the biogenic synthesis of extracellular metal nanoparticles by peptides, bacteria, fungi, and plants. *Appl. Microbiol. Biotechnol.* **2011**, *90*, 1609−1624.
(26) Jain, N.; Bhargava, A.; Tarafdar, J. C.; Singh, S. K.; Panwar, J. A biomimetic approach towards synthesis of zinc oxide nanoparticles. *Appl. Microbiol. Biotechnol.* **2013**, *97*, 859−869.
(27) Nagao, T.; Inoue, S.; Yoshimi, F.; Sodeyama, M.; Omori, Y.; Mizuta, T.; Kawano, N.; Morioka, Y. Postoperative recurrence of hepatocellular carcinoma. *Ann. Surg.* **1990**, *211*, 28−33.
(28) Nagasue, N.; Uchida, M.; Makino, Y.; Takemoto, Y.; Yamanoi, A.; Hayashi, T.; Chang, Y.-C.; Kohno, H.; Nakamura, T.; Yukaya, H. Incidence and factors associated with intrahepatic recurrence following resection of hepatocellular carcinoma. *Gastroenterology* **1993**, *105*, 488−488.
(29) Bielack, S. S.; Carrle, D.; Hardes, J.; Schuck, A.; Paulussen, M. Bone tumors in adolescents and young adults. *Curr. Treat. Options Oncol.* **2008**, *9*, 67−80.
(30) Hughes, D. P. Strategies for the targeted delivery of therapeutics for osteosarcoma. *Expert Opin. Drug Delivery* **2009**, *6*, 1311−1321.
(31) Bhargava, A.; Jain, N.; Khan, M. A.; Pareek, V.; Dilip, R. V.; Panwar, J. Utilizing metal tolerance potential of soil fungus for efficient synthesis of gold nanoparticles with superior catalytic activity for degradation of rhodamine B. *J. Environ. Manage.* **2016**, *183*, 22−32.
(32) Laemmli, U. K. Cleavage of structural proteins during the assembly of the head of bacteriophage T4. *Nature* **1970**, *227*, 680−685.
(33) Chowdhury, R.; Chowdhury, S.; Roychoudhury, P.; Mandal, C.; Chaudhuri, K. Arsenic induced apoptosis in malignant melanoma cells is enhanced by menadione through ROS generation, p38 signaling and p53 activation. *Apoptosis* **2009**, *14*, 108−123.
(34) Pasha, S. S.; Das, P.; Rath, N. P.; Bandyopadhyay, D.; Jana, N. R.; Laskar, I. R. Water soluble luminescent cyclometalated platinum (II) complex—A suitable probe for bio-imaging applications. *Inorg. Chem. Commun.* **2016**, *67*, 107−111.
(35) Biederbick, A.; Kern, H.; Elsässer, H. Monodansylcadaverine (MDC) is a specific in vivo marker for autophagic vacuoles. *Eur. J. Cell Biol.* **1995**, *66*, 3−14.
(36) Munafó, D. B.; Colombo, M. I. A novel assay to study autophagy: regulation of autophagosome vacuole size by amino acid deprivation. *J. Cell Sci.* **2001**, *114*, 3619−3629.
(37) Gurunathan, S.; Han, J. W.; Eppakayala, V.; Jeyaraj, M.; Kim, J.-H. Cytotoxicity of biologically synthesized silver nanoparticles in MDA-MB-231 human breast cancer cells. *BioMed Res. Int.* **2013**, *2013*, No. 535796.
(38) Palvai, S.; Nagraj, J.; Mapara, N.; Chowdhury, R.; Basu, S. Dual drug loaded vitamin D3 nanoparticle to target drug resistance in cancer. *RSC Adv.* **2014**, *4*, 57271−57281.
(39) Gurunathan, S.; Kalishwaralal, K.; Vaidyanathan, R.; Venkataraman, D.; Pandian, S. R. K.; Muniyandi, J.; Hariharan, N.; Eom, S. H. Biosynthesis, purification and characterization of silver nanoparticles using Escherichia coli. *Colloids Surf., B* **2009**, *74*, 328−335.
(40) Ge, L.; Li, Q.; Wang, M.; Ouyang, J.; Li, X.; Xing, M. M. Nanosilver particles in medical applications: synthesis, performance, and toxicity. *Int. J. Nanomed.* **2014**, *9*, 2399−2407.
(41) Ingale, A. G.; Chaudhari, A. Biogenic synthesis of nanoparticles and potential applications: An eco-friendly approach. *J. Nanomed. Nanotechnol.* **2013**, *4*, 1−7.
(42) Satyavani, K.; Gurudeeban, S.; Ramanathan, T.; Balasubramanian, T. Biomedical potential of silver nanoparticles synthesized from calli cells of *Citrullus colocynthis* (L.) Schad. *J. Nanobiotechnol.* **2011**, *9*, 1−8.
(43) Babu, A.; Amreddy, N.; Ramesh, R. Nanoparticle-based cisplatin therapy for cancer. *Ther. Delivery* **2015**, *6*, 115−119.
(44) Wang, X.; Song, P.; Peng, L.; Tong, A.; Xiang, Y. Aggregation-Induced Emission Luminogen-Embedded Silica Nanoparticles Containing DNA Aptamers for Targeted Cell Imaging. *ACS Appl. Mater. Interfaces* **2016**, *8*, 609−616.

DOI: 10.1021/acsomega.7b00045
ACS Omega 2017, 2, 1489−1504

(45) Sharma, V.; Anderson, D.; Dhawan, A. Zinc oxide nanoparticles induce oxidative DNA damage and ROS-triggered mitochondria mediated apoptosis in human liver cells (HepG2). *Apoptosis* **2012**, *17*, 852−870.
(46) Zhu, B.; Li, Y.; Lin, Z.; Zhao, M.; Xu, T.; Wang, C.; Deng, N. Silver nanoparticles induce HePG-2 cells apoptosis through ROS-mediated signaling pathways. *Nanoscale Res. Lett.* **2016**, *11*, 198−206.
(47) Wang, J.; Deng, X.; Zhang, F.; Chen, D.; Ding, W. ZnO nanoparticle-induced oxidative stress triggers apoptosis by activating JNK signaling pathway in cultured primary astrocytes. *Nanoscale Res. Lett.* **2014**, *9*, 117.
(48) Akhtar, M. J.; Alhadlaq, H. A.; Kumar, S.; Alrokayan, S. A.; Ahamed, M. Selective cancer-killing ability of metal-based nanoparticles: implications for cancer therapy. *Arch. Toxicol.* **2015**, *89*, 1895−1907.
(49) Manke, A.; Wang, L.; Rojanasakul, Y. Mechanisms of nanoparticle-induced oxidative stress and toxicity. *BioMed. Res. Int.* **2013**, *2013*, No. 942916.
(50) Chou, A. J.; Gorlick, R. Chemotherapy resistance in osteosarcoma: current challenges and future directions. *Expert Rev. Anticancer Ther.* **2006**, *6*, 1075−1085.
(51) Marano, F.; Hussain, S.; Rodrigues-Lima, F.; Baeza-Squiban, A.; Boland, S. Nanoparticles: molecular targets and cell signalling. *Arch. Toxicol.* **2011**, *85*, 733−741.
(52) Satapathy, S. R.; Mohapatra, P.; Das, D.; Siddharth, S.; Kundu, C. N. The apoptotic effect of plant based nanosilver in colon cancer cells is a p53 dependent process involving ROS and JNK cascade. *Pathol. Oncol. Res.* **2015**, *21*, 405−411.
(53) Mao, B.-H.; Tsai, J.-C.; Chen, C.-W.; Yan, S.-J.; Wang, Y.-J. Mechanisms of silver nanoparticle-induced toxicity and important role of autophagy. *Nanotoxicology* **2016**, *10*, 1021−1040.
(54) Zhang, Z.; Zhou, L.; Zhou, Y.; Liu, J.; Xing, X.; Zhong, J.; Xu, G.; Kang, Z.; Liu, J. Mitophagy induced by nanoparticle−peptide conjugates enabling an alternative intracellular trafficking route. *Biomaterials* **2015**, *65*, 56−65.
(55) Jeong, J.-K.; Gurunathan, S.; Kang, M.-H.; Han, J. W.; Das, J.; Choi, Y.-J.; Kwon, D.-N.; Cho, S.-G.; Park, C.; Seo, H. G. Hypoxia-mediated autophagic flux inhibits silver nanoparticle-triggered apoptosis in human lung cancer cells. *Sci. Rep.* **2016**, *6*, No. 21688.
(56) Castiglioni, S.; Cazzaniga, A.; Perrotta, C.; Maier, J. A. Silver nanoparticles-induced cytotoxicity requires ERK activation in human bladder carcinoma cells. *Toxicol. Lett.* **2015**, *237*, 237−243.
(57) Rinna, A.; Magdolenova, Z.; Hudecova, A.; Kruszewski, M.; Refsnes, M.; Dusinska, M. Effect of silver nanoparticles on mitogen-activated protein kinases activation: role of reactive oxygen species and implication in DNA damage. *Mutagenesis* **2015**, *30*, 59−66.
(58) Duan, H.; Wang, D.; Li, Y. Green chemistry for nanoparticle synthesis. *Chem. Soc. Rev.* **2015**, *44*, 5778−5792.

DOI: 10.1021/acsomega.7b00045
ACS Omega 2017, 2, 1489−1504